

Online randomized interpolative decomposition with *a posteriori* error estimator for temporal PDE data reduction

Angran Li^a, Stephen Becker^b, Alireza Doostan^{a,*}

^a*Smead Aerospace Engineering Sciences, University of Colorado Boulder, 80309, Boulder, USA*

^b*Applied Mathematics, University of Colorado Boulder, 80309, Boulder, USA*

Abstract

Traditional low-rank approximation is a powerful tool to compress the huge data matrices that arise in simulations of partial differential equations (PDE), but suffers from high computational cost and requires several passes over the PDE data. The compressed data may also lack interpretability thus making it difficult to identify feature patterns from the original data. To address this issue, we present an online randomized algorithm to compute the interpolative decomposition (ID) of large-scale data matrices *in situ*. Compared to previous randomized IDs that used the QR decomposition to determine the column basis, we adopt a streaming ridge leverage score-based column subset selection algorithm that dynamically selects proper basis columns from the data and thus avoids an extra pass over the data to compute the coefficient matrix of the ID. In particular, we adopt a single-pass error estimator based on the non-adaptive Hutch++ algorithm to provide real-time error approximation for determining the best coefficients. As a result, our approach only needs a single pass over the original data and thus is suitable for large and high-dimensional matrices stored outside of core memory or generated in PDE simulations. We also provide numerical experiments on turbulent channel flow and ignition simulations, and on the NSTX Gas Puff Image dataset, comparing our algorithm with the offline ID algorithm to demonstrate its utility in real-world applications.

Keywords: Low-rank Approximation, Single-pass Algorithm, Interpolative Decomposition, Column Subset Selection, Randomized Algorithm

1. Introduction

Recent advances in parallel computing have led to an increasing interest in addressing challenges in industrial application, scientific design, and discovery using computer simulations. In particular, simulations based on partial differential equations (PDEs) have grown in size and complexity, and generate a considerable amount of data at fast rates. However, the speed of the current input/output (I/O) filesystem does not keep up with the data generation speed thus limiting the improvement of computation time. It is also challenging to store the entire simulation data due to the storage size limitation of current filesystems. Therefore, it is essential to develop compression algorithms that can efficiently reduce the size of large PDE data streams for storage or visualization.

Our setup is that $\mathbf{A} = [\mathbf{a}_1, \dots, \mathbf{a}_n]$ is a $m \times n$ matrix that contains n snapshots of the PDE solution, each of size m , i.e., \mathbf{a}_t is the discretized solution at some discrete time step t . We are most interested in the case when \mathbf{A} is so large that it is impossible to store all at once in the main memory of a computer, and we receive incremental updates of new columns after discarding old columns, as in a

*Corresponding author. E-mail: alireza.doostan@colorado.edu.

time-dependent PDE simulation. We also assume $m \geq n$, as if there are very many time steps n , we work with a smaller block of time and just repeat the approximation procedures every block.

Traditionally, low-rank approximation has served as a robust and powerful tool for data compression tasks. The goal of low-rank approximation is to find a rank k matrix that is as close as possible to \mathbf{A} with distance typically measured using the spectral or Frobenius norms. The Eckart-Young theorem [1] states that the best rank- k approximation of \mathbf{A} in the spectral or Frobenius norm can be provided via the singular value decomposition (SVD):

$$\mathbf{A} \approx \mathbf{U}_k \mathbf{\Sigma}_k \mathbf{V}_k^T, \quad (1)$$

where $\mathbf{\Sigma}_k$ is a diagonal matrix whose entries are the k largest singular values of \mathbf{A} , and \mathbf{U}_k and \mathbf{V}_k contain the first k left and right singular vectors, respectively. Instead of storing the mn numbers of \mathbf{A} , the rank k matrices $\mathbf{U}_k, \mathbf{\Sigma}_k, \mathbf{V}_k$ can be stored with only $k(m + n + 1)$ numbers and thus achieves compression of \mathbf{A} ; variants of this approach that also further compress $\mathbf{U}_k, \mathbf{\Sigma}_k, \mathbf{V}_k$ have been proposed in the literature, e.g., [2]. However, it is challenging for the SVD to tackle large matrices due to its expensive computational cost in both time and memory. Although the high cost can be reduced using iterative algorithms, such as the power method or Krylov methods, these methods require access to the matrix multiple times so they are not suitable for a streaming scenario.

The interpolative decomposition (ID) is another low-rank approximation approach that uses a submatrix of \mathbf{A} (a subset of its rows or columns) as the basis to approximate the original data. Though the ID is generally less accurate than the SVD [3], the decomposition results are more interpretable since it utilizes a subset of \mathbf{A} as basis vectors to approximate the original matrix. For matrices with important properties such as sparsity or non-negativity, one can specifically select bases that preserve these properties and while still obtaining a compact representation of the original data. The ID method has been applied in compressing computational fluid dynamics data [4, 5] and computational electromagnetic problems [6, 7], as well as in multi-fidelity uncertainty quantification [8, 9, 10]. The idea of column ID is to approximate the matrix \mathbf{A} as a product of a subset of its columns (also called a column skeleton) $\mathbf{A}(:, \mathcal{J})$, with \mathcal{J} containing a subset of k indices from $\{1, 2, \dots, n\}$, and a coefficient matrix $\mathbf{P} \in \mathbb{R}^{k \times n}$ which reconstructs the matrix via

$$\mathbf{A} \approx \mathbf{A}(:, \mathcal{J})\mathbf{P}, \quad (2)$$

where we use MATLAB notation to specify submatrices. A standard way to obtain the ID of \mathbf{A} is to first compute the column-pivoted QR (CPQR) factorization of \mathbf{A} and use the top k pivot indices to obtain \mathcal{J} , and then compute \mathbf{P} by minimizing the Frobenius norm $\|\mathbf{A} - \mathbf{A}(:, \mathcal{J})\mathbf{P}\|_F^2$. However, the CPQR factorization requires multiple passes over \mathbf{A} , and thus ID shares a similar issue as SVD in handling large-size matrices.

Randomized methods based on Johnson-Lindenstrauss random projection [11, 12, 13] have garnered significant attention for their capability to handle the low-rank approximation of large matrices with reduced cost and fewer passes. They can also output a low-rank approximation with a $(1 + \epsilon)$ factor of the optimal error when measured using the Frobenius norm and thus have strong theoretical guarantees to ensure that the approximation error is controlled, making them suitable for applications where accuracy is critical. In this study, we are specifically interested in the randomized ID method [11]. The key idea is first to use random projection to create a sketch matrix $\mathbf{S} \in \mathbb{R}^{\ell \times n}$ ($\ell \ll m$) as

$$\mathbf{S} = \mathbf{\Omega}\mathbf{A} = [\mathbf{\Omega}\mathbf{a}_1, \dots, \mathbf{\Omega}\mathbf{a}_n], \quad (3)$$

where $\mathbf{\Omega} \in \mathbb{R}^{\ell \times m}$ is the random projection matrix and \mathbf{S} can be treated as a spanning set for the range of a matrix \mathbf{A} . If ℓ is sufficiently small, then \mathbf{S} can be stored all at once in main memory, unlike

\mathbf{A} , and since $\mathbf{\Omega}$ can be applied to each column of \mathbf{A} , the random projection can be computed on streaming data. Then, CPQR is applied to \mathbf{S} to obtain the k column indices in \mathcal{J} as well as the column skeleton $\mathbf{A}(:, \mathcal{J})$. Finally, the coefficient matrix \mathbf{P} can be computed by minimizing $\|\mathbf{A} - \mathbf{A}(:, \mathcal{J})\mathbf{P}\|_F^2$. These last two steps can be combined in a single pass, but this is still in addition to the first pass to compute \mathbf{S} , so overall this is a two-pass method. Compared to traditional, deterministic methods, the randomized ID algorithm is pass-efficient and it also reduces the time and space complexity for computing the coefficient matrix since the CPQR is applied to the smaller sketch matrix and involves fewer floating-point operations (*flops*). However, the difference between two passes and one pass is great: the two-pass randomized ID method still needs either an extra simulation run to obtain the column basis or saving data to secondary or tertiary memory. Hence, our motivation in this paper is to develop an online method that collects the column skeleton and computes the coefficient matrix in a single pass.

We note that a closely related method, column subset selection (CSS), has been explored in previous work to identify a subset of columns that serves as the optimal basis to depict the original matrix [14, 15, 16, 17, 18, 19, 20]. In more detail, given a matrix \mathbf{A} , CSS aims to find a small subset \mathbf{C} of its columns that minimizes the projection error of the matrix to the span of the selected columns:

$$\min_{\mathbf{X}} \|\mathbf{C}\mathbf{X} - \mathbf{A}\|_F^2 = \|\mathbf{C}\mathbf{C}^\dagger \mathbf{A} - \mathbf{A}\|_F^2, \quad (4)$$

where \mathbf{C}^\dagger denotes the pseudoinverse of \mathbf{C} . The CSS and ID problems are similar since \mathbf{C} comes from \mathbf{A} and one possible ID solution can be obtained by setting $\mathbf{A}(:, \mathcal{J}) = \mathbf{C}$ and $\mathbf{P} = \mathbf{X}$. In [21, 22], the authors developed online CSS algorithms using residual norm and ridge leverage score-based random sampling which only require one pass through the data. However, most online CSS methods only provide the column subset but still need an extra pass over the entire data to build the coefficient matrix for reconstruction. In this regard, the randomized and online CSS algorithms complement each other well since the randomized algorithm can efficiently compute the coefficients using the sketch matrix given the selected column basis from the online CSS. This inspires us to combine both algorithms in a single framework and develop an online algorithm to handle the streaming data and obtain the ID matrices in one PDE simulation run.

1.1. Contributions

In this study, we focus on addressing data compression in large-scale PDE simulations where the PDE solution at each time step arrives in a streaming fashion. The main contribution of this paper is the development of a novel online randomized column ID approach to perform temporal compression of large-scale simulation data. In particular, we make the following contributions:

- Extending on the ridge leverage score-based CSS method to compute the column basis in one pass [21], we use a random projection sketching technique to simultaneously compute the coefficient matrix without any additional passes through the data;
- We consider four different approaches to compute the coefficients and adaptively choose the best one by evaluating the approximation error of different coefficients. Specifically, a single-pass error estimator based on the non-adaptive Hutch++ (NA-Hutch++) algorithm [23] is adopted to provide real-time error approximation for determining the best coefficients;
- To accommodate datasets where the reconstruction accuracy of the gradient field is important, we also derive a fast gradient estimation and use the gradient information in both CSS and coefficient computation processes;

- Demonstrate the effectiveness of our approach by evaluating the compression performance of time-dependent scientific data obtained from several applications, namely the direct numerical simulation of a turbulent channel flow [24, 25, 26], an ignition simulation, and the NSTX Gass Puff Image (GPI) data [27, 28, 29].

The remainder of the manuscript is organized as follows. In Section 2, we provide appropriate background and context for the randomized ID and review two online CSS algorithms using residual-based and ridge leverage score-based sampling, respectively. In Section 3, we outline the online randomized ID algorithm proposed in this work. In Section 4, we present the numerical experiments for the proposed method applied to three different simulation datasets. Finally, in Section 5, we summarize the findings of this work and suggest future research.

2. Background

In this section, we review the standard CPQR-based ID and online residual-based CSS algorithms that are used to build our algorithm. We use the following notation. Matrices and vectors are denoted by capital and lowercase bold letters, respectively. The j^{th} column of \mathbf{A} is expressed as \mathbf{a}_j and the $(i, j)^{\text{th}}$ entry of \mathbf{A} as a_{ij} . For a matrix \mathbf{A} , using MATLAB notation, the submatrix $\mathbf{A}(:, \mathcal{J}) = \mathbf{A}_{\mathcal{J}}$ represents those columns from \mathbf{A} with indices given by the set \mathcal{J} . \mathbf{A}^\dagger denotes the Moore-Penrose inverse of \mathbf{A} . The symbol \mathbf{A}_k denotes the best rank- k approximation of \mathbf{A} with respect to the Frobenius norm. In general, \mathbf{C} denotes the selected column subset, equivalent to $\mathbf{A}_{\mathcal{J}}$, while $\mathbf{\Omega}$ denotes the random projection matrix, and \mathbf{S} denotes the matrix sketch of \mathbf{A} , $\mathbf{S} = \mathbf{\Omega}\mathbf{A}$.

2.1. ID based on CPQR

We first review the computation of low-rank column ID via CPQR factorization, which is later used as the benchmark to evaluate the performance of our algorithm. The column pivoted (thin/reduced) QR factorization of $\mathbf{A} \in \mathbb{R}^{m \times n}$ (assuming $m \geq n$) returns

$$\mathbf{AZ} = \mathbf{QR}, \quad (5)$$

where \mathbf{Z} is a permutation matrix, $\mathbf{Q} \in \mathbb{R}^{m \times n}$ has orthogonal columns and $\mathbf{R} \in \mathbb{R}^{n \times n}$ is an upper triangular matrix. \mathbf{Q} and \mathbf{R} can be partitioned into blocks such that

$$\mathbf{Q} = [\mathbf{Q}_k \quad \mathbf{Q}_{n-k}], \quad (6)$$

$$\mathbf{R} = \begin{bmatrix} \mathbf{R}_{11} & \mathbf{R}_{12} \\ \mathbf{0} & \mathbf{R}_{22} \end{bmatrix}, \quad (7)$$

where $k < \min(m, n)$, $\mathbf{Q}_k \in \mathbb{R}^{m \times k}$ contains the first k orthogonal columns of \mathbf{A} , $\mathbf{Q}_{n-k} \in \mathbb{R}^{m \times (n-k)}$, $\mathbf{R}_{11} \in \mathbb{R}^{k \times k}$, $\mathbf{R}_{12} \in \mathbb{R}^{k \times (n-k)}$, and $\mathbf{R}_{22} \in \mathbb{R}^{(n-k) \times (n-k)}$. The rank k approximation of \mathbf{A} is obtained from the reduced CPQR as

$$\mathbf{AZ} \approx \mathbf{Q}_k [\mathbf{R}_{11} \quad \mathbf{R}_{12}] \quad (8)$$

$$= \mathbf{Q}_k \mathbf{R}_{11} [\mathbf{I}_k \quad \mathbf{R}_{11}^{-1} \mathbf{R}_{12}]. \quad (9)$$

Letting the index set \mathcal{J} point to the first k pivoted vectors of \mathbf{A} , we have

$$\mathbf{A}_{\mathcal{J}} = \mathbf{Q}_k \mathbf{R}_{11}, \quad (10)$$

$$\mathbf{A} \approx \mathbf{A}_{\mathcal{J}} [\mathbf{I}_k \quad \mathbf{R}_{11}^{-1} \mathbf{R}_{12}] \mathbf{Z}^T. \quad (11)$$

The column ID of $\mathbf{A} \approx \mathbf{A}_{\mathcal{J}} \mathbf{P}$ is obtained by setting $\mathbf{P} = [\mathbf{I}_k \quad \mathbf{R}_{11}^{-1} \mathbf{R}_{12}] \mathbf{Z}^T$, which is equivalent to compute \mathbf{P} by minimizing $\|\mathbf{A} - \mathbf{A}(:, \mathcal{J})\mathbf{P}\|_F^2$.

2.2. Review of online CSS algorithms

To develop an online ID method, it is crucial to simultaneously determine the column basis and compute the current coefficient matrix in a streaming setting. Both *online* and *streaming* CSS methods are promising since they each make decisions on the column as it arrives, leading to the selected columns being immediately used to compute a coefficient matrix without another pass through the data. Therefore, we consider *online* and *streaming* to be equivalent terms and use them interchangeably throughout this paper. In the following sections, we provide a review of two online CSS algorithms using residual-based and ridge leverage score-based sampling, respectively.

2.2.1. Online CSS using residual-based sampling

We first review an online CSS algorithm using residual-based sampling proposed in [22]. The basic idea is to maintain a subspace corresponding to the span of previously selected columns while collecting new columns based on their residual norm by projecting to the subspace. The arriving sequence of columns is partitioned into steps where we update the column subset until the residual norm based on the current column subset reaches a threshold. To describe the method, we first denote the previously and currently selected column subsets as \mathbf{C}_{pre} and $\mathbf{C}_{\text{current}}$, respectively. $\Pi_{\mathbf{C}}^\perp$ denotes the orthogonal projection onto the subspace orthogonal to the column space of \mathbf{C} , and σ denotes the “residual mass” that measures the accumulated normalized residual of approximating new data columns with the currently selected columns in each CSS step. The algorithm takes the data matrix \mathbf{A} , an estimate of the target rank k , and a parameter satisfying $\xi \geq \|\mathbf{A} - \mathbf{A}_k\|_F^2$ as input. Both \mathbf{C}_{pre} and $\mathbf{C}_{\text{current}}$ are initialized to the empty set, and σ is set to 0. When a new data column \mathbf{a} arrives, we first compute its probability to be selected into the subset $\mathbf{C}_{\text{current}}$ as

$$p_a := \frac{k \|\Pi_{\mathbf{C}_{\text{pre}}}^\perp \mathbf{a}\|_2^2}{\xi}. \quad (12)$$

This new column is then added to $\mathbf{C}_{\text{current}}$ with probability $\min(p_a, 1)$. The probability p_a is also added to σ as a collection of residual mass in this step. The process continues until $p_a \geq 1$ or $\sigma \geq 1$, indicating that the residual norm of using the current subset to approximate the new observed columns reaches the error threshold. Therefore, the previously selected columns \mathbf{C}_{pre} are not sufficient to provide an accurate approximation of the new columns observed in this step, and thus an update with the newly selected columns $\mathbf{C}_{\text{current}}$ is performed:

$$\mathbf{C}_{\text{pre}} \leftarrow \mathbf{C}_{\text{pre}} \cup \mathbf{C}_{\text{current}}. \quad (13)$$

Note that \mathbf{C}_{pre} is not updated unless it has built up enough residual mass σ , and thus σ can be used to bound the number of selected columns [22]. At this point, $\sigma = 0$ and $\mathbf{C}_{\text{current}} = \emptyset$ are reset to start a new step of collection columns. The process continues until the entire data matrix is loaded to obtain the CSS of \mathbf{A} with selected columns \mathbf{C} and indices \mathcal{J} . As proved in [22], with probability $\geq 1 - \delta$, the algorithm provides a subset \mathbf{C} such that

$$\|\Pi_{\mathbf{C}}^\perp \mathbf{A}\|_F^2 \leq \xi \cdot \mathcal{O}\left(\log \frac{\|\mathbf{A}\|_F^2}{\xi} + \frac{\log(1/\delta)}{k}\right), \quad (14)$$

and thus we can often expect the probability $p_a \leq 1$.

The selected columns can then be used as the basis to compute the coefficient matrix \mathbf{P} and obtain the column ID of \mathbf{A} as $\mathbf{A} \approx \mathbf{C}\mathbf{P}$. The coefficient computation methods will be explained in Section 3.2. The detailed implementation of the online CSS is described in Algorithm 1. In Step 10, we notice that the selected columns \mathbf{C} keep expanding without replacement and thus the algorithm may not be suitable for performing CSS with a fixed-size subset.

Algorithm 1: Online CSS using residual-based sampling [22]

Input: Data matrix $\mathbf{A}_{m \times n}$, target rank k , parameter ξ

- 1 Initialize $\mathbf{C}_{\text{pre}} = \emptyset$, $\mathbf{C}_{\text{current}} = \emptyset$ and $\sigma = 0$
- 2 **while** A is not completely read through **do**
- 3 Read next column of \mathbf{A} , denoted by \mathbf{a} , into RAM
- 4 Let $p_a := \frac{k \|\Pi_{\mathbf{C}_{\text{pre}}}^\perp \mathbf{a}\|_2^2}{\xi}$.
- 5 With probability $\min(p_a, 1)$, add \mathbf{a} to $\mathbf{C}_{\text{current}}$
- 6 **if** $p_a < 1$ **then**
- 7 Increment $\sigma \leftarrow \sigma + p_a$
- 8 **end**
- 9 **if** $p_a \geq 1$ or $\sigma \geq 1$ **then**
- 10 Set $\mathbf{C}_{\text{pre}} \leftarrow \mathbf{C}_{\text{pre}} \cup \mathbf{C}_{\text{current}}$ and reset $\sigma = 0$ and $\mathbf{C}_{\text{current}} = \emptyset$
- 11 **end**
- 12 **end**

Output: $\mathbf{C} = \mathbf{C}_{\text{pre}} \cup \mathbf{C}_{\text{current}}$

2.2.2. Streaming ridge leverage score based CSS

In [21], Cohen *et al.* proposed a streaming CSS algorithm via ridge leverage score sampling. The idea is to select columns using non-uniform probabilities determined by ridge leverage score. The leverage score of the j th column \mathbf{a}_j of \mathbf{A} is defined as:

$$\tau_j = \mathbf{a}_j^T (\mathbf{A} \mathbf{A}^T)^\dagger \mathbf{a}_j, \quad (15)$$

where τ_j measures how important \mathbf{a}_j is in composing the range of \mathbf{A} . It is maximized at 1 when \mathbf{a}_j is linearly independent of the other columns of \mathbf{A} and decreases when many other columns approximately align with \mathbf{a}_j . In practice, the rank- k leverage score can be computed with respect to the rank- k approximation \mathbf{A}_k of \mathbf{A} to quickly approximate the scores. However, \mathbf{A}_k is not always unique and the low-rank leverage score is sensitive to matrix perturbation which largely limits its ability to obtain accurate scores for sampling. To resolve this issue, the ridge *leverage* score is defined by adding a regularization term to Eq. (15),

$$\tau_j = \mathbf{a}_j^T (\mathbf{A} \mathbf{A}^T + \lambda \mathbf{I})^\dagger \mathbf{a}_j, \quad (16)$$

where we set $\lambda = \|\mathbf{A} - \mathbf{A}_k\|_F^2 / k$. By adding $\lambda \mathbf{I}$ to $\mathbf{A} \mathbf{A}^T$, the effect of smaller singular directions is alleviated, leading to smaller sampling probabilities for them. As shown in [21], the ridge leverage score-based CSS satisfies the error bound

$$\|\mathbf{A} - (\mathbf{C} \mathbf{C}^\dagger \mathbf{A})_k\|_F^2 \leq (1 + \epsilon) \|\mathbf{A} - \mathbf{A}_k\|_F^2, \quad (17)$$

where \mathbf{C} is the selected subset of \mathbf{A} 's columns, $(\mathbf{C} \mathbf{C}^\dagger \mathbf{A})_k$ is a rank- k matrix in the column span of \mathbf{C} .

In the streaming CSS settings, the storage limit for the loaded columns is assumed to be t . The basic idea of the algorithm is that whenever t columns are loaded into RAM, the ridge leverage score for each column is computed and used to update the selected columns based on the score.

Lemma 1. [21] (*Monotonicity of ridge leverage score*). For any $\mathbf{A} \in \mathbb{R}^{m \times n}$ and vector $\mathbf{b} \in \mathbb{R}^m$, for every $j \in 1, 2, \dots, n$ we have

$$\tau_j(\mathbf{A}) \leq \tau_j(\mathbf{A} \cup \mathbf{b}), \quad (18)$$

where $\mathbf{A} \cup \mathbf{b}$ denotes the column \mathbf{b} appended to \mathbf{A} as the final column.

Based on the monotonicity of the ridge leverage score (Lemma 1), whenever a new column is added to the original matrix, the ridge leverage scores of the already observed columns only decrease, which ensures that the previously selected columns are not biased with larger scores due to their earlier observation and thus newly observed columns can also be selected into the column subset. To ensure this monotonicity property holds for the low-rank leverage scores, where λ depends on \mathbf{A} , a generalized ridge leverage score of $\mathbf{A} \in \mathbb{R}^{m \times n}$ with respect to any matrix $\mathbf{B} \in \mathbb{R}^{m \times n_B}$ is defined in [21] as

$$\tau_i^{\mathbf{B}}(\mathbf{A}) = \begin{cases} \mathbf{a}_i^T \left(\mathbf{B}\mathbf{B}^T + \frac{\|\mathbf{B} - \mathbf{B}_k\|_F^2}{k} \mathbf{I} \right)^\dagger \mathbf{a}_i & \text{for } \mathbf{a}_i \in \text{span} \left(\mathbf{B}\mathbf{B}^T + \frac{\|\mathbf{B} - \mathbf{B}_k\|_F^2}{k} \mathbf{I} \right), \\ \infty & \text{otherwise.} \end{cases} \quad (19)$$

The generalized monotonicity bound of Eq. (19) has been proven in [21]. In the streaming CSS process, \mathbf{B} is chosen as the *frequent-directions* [30] sketch of \mathbf{A} . The frequent-directions algorithm maintains the invariant that the last column of \mathbf{B} is always all-zero valued. When a new column from the input matrix \mathbf{A} is observed, it replaces the all-zero valued column of \mathbf{B} . Then, the last column of \mathbf{B} is nullified by a two-stage process. First, the sketch is rotated using its SVD such that its columns are orthogonal and in descending magnitude order. Then, the sketch columns norms are “shrunk” so that at least one of them is set to zero. The algorithm produces the \mathbf{B} satisfying

$$\mathbf{B}\mathbf{B}^T \prec \mathbf{A}\mathbf{A}^T \quad \text{and} \quad \|\mathbf{A}\mathbf{A}^T - \mathbf{B}\mathbf{B}^T\|_2 \leq 2\|\mathbf{A}\|_F^2/n_B. \quad (20)$$

At the beginning of the CSS process, $\mathbf{C} = \mathbf{0}_{m \times t}$, $\mathbf{D} = \mathbf{0}_{m \times t}$ matrices are initialized to store currently selected columns and new data columns, respectively. The vector $[\tau_1^{\text{old}}, \dots, \tau_t^{\text{old}}] = \mathbf{1}$ is also initialized to store the ridge leverage score of \mathbf{C} with respect to the already observed data columns. With the arrival of the data sequence, \mathbf{D} and the frequent-directions sketch \mathbf{B} are first updated using every new data column until t columns are read. The ridge leverage scores for new columns in \mathbf{D} ($\tau^{\mathbf{D}}$) and previously selected columns \mathbf{C} (τ) with respect to the updated sketch \mathbf{B} are computed using Eq. (23), respectively. Then, the normalized leverage score is used as the probability for selecting new columns and updating \mathbf{C} . For the i^{th} column in \mathbf{C} , if the ridge leverage score τ_i decreases compared to τ_i^{old} , we will discard that column with a probability equal to the proportion that its ridge leverage score decreased by, otherwise, the column is kept in the subset. If the column is discarded, we will select a new column from \mathbf{D} based on the ridge leverage score $\tau^{\mathbf{D}}$. This process is similar to the reservoir sampling [?] in that at any point in the stream, we have a set of columns sampled using true ridge scores concerning the currently observed matrix as the universal criteria. The error and complexity of the streaming ridge leverage score-based CSS is proved in [21] as the following theorem:

Theorem 1. (*Streaming column subset selection*) [21] *Algorithm 2 achieves computing a $(1+\epsilon)$ error column subset \mathbf{C} with $\mathcal{O}(k \log k + k \log(1/\delta)/\epsilon)$ columns in a single-pass over \mathbf{A} . The algorithm uses $\mathcal{O}(nk)$ space in addition to the space required to store the subset and succeeds with probability $1 - \delta$.*

Algorithm 2: Streaming CSS based on ridge leverage score

Input: Data matrix $\mathbf{A}_{m \times n}$, target rank k , basis size t , accuracy ϵ , success probability $(1 - \delta)$

Output: Selected columns $\mathbf{C}_{m \times t}$

```
1 Initialize the Frobenius norm of the observed data matrix as  $\|\mathbf{A}_{obs}\|_F^2 = 0$ 
2 Set  $count = 0$ ,  $\mathbf{C} = \mathbf{0}_{m \times t}$ ,  $\mathbf{D} = \mathbf{0}_{m \times t}$ 
3 Set the index set for the basis columns and new columns as  $\mathcal{J}^C, \mathcal{J}^D \leftarrow \mathbf{0}_{t \times 1}$ 
4 Initialize  $[\tau_1^{old}, \dots, \tau_t^{old}] = 1$  for storing ridge leverage scores of  $\mathbf{C}$  with respect to previous read
   data columns.
5 for  $j = 1, \dots, n$  do
6   Read the next column  $j$  of  $\mathbf{A}$  into RAM, denoted by  $\mathbf{a}_j$ 
7    $\mathbf{B} = \text{FrequentDirections}(\mathbf{B}, \mathbf{a}_j)$ 
8   if  $count < t$  then
9      $\mathbf{d}_{count} = \mathbf{a}_j$ ,  $\mathcal{J}_{count}^D = j$ ,  $\|\mathbf{A}_{obs}\|_F^2 \leftarrow \|\mathbf{A}_{obs}\|_F^2 + \|\mathbf{a}_j\|_2^2$ ,  $count \leftarrow count + 1$ 
10  else
11    Update leverage scores of columns in  $\mathbf{C}$  as
12     $[\tau_1, \dots, \tau_t] = \min\{[\tau_1^{old}, \dots, \tau_t^{old}], \text{ApproximateRidgeScores}(\mathbf{B}, \mathbf{C}, \|\mathbf{A}_{obs}\|_F^2)\}$ 
13    Approximate leverage scores of new columns in  $\mathbf{D}$  as
14     $[\tau_1^D, \dots, \tau_t^D] = \text{ApproximateRidgeScores}(\mathbf{B}, \mathbf{D}, \|\mathbf{A}_{obs}\|_F^2)$ 
15    for  $i = 1, \dots, t$  do
16      if  $c_i \neq 0$  then
17        With probability  $(1 - \tau_i / \tau_i^{old})$ , set  $c_i = 0$ ,  $\tau_i^{old} = 1$  and  $\mathcal{J}_i^C = 0$ 
18        Otherwise set  $\tau_i^{old} = \tau_i$ 
19      end
20      if  $c_i = 0$  then
21        for  $r = 1, \dots, t$  do
22          With probability  $\frac{\tau_r^D c(k \log k + k \log(1/\delta)/\epsilon)}{t}$ , set  $c_i = \mathbf{d}_r$ ,  $\tau_i^{old} = \tau_r^D$  and
23           $\mathcal{J}_i^C = \mathcal{J}_r^D$ 
24        end
25      end
26    end
27     $count = 0$ 
28  end
29 end
30 Function FrequentDirections( $\mathbf{B}, \mathbf{a}_j$ ):
31   // Follow the idea in [30] to update  $\mathbf{B}$ 
32   Replace the  $n_B^{\text{th}}$  all-zero valued column of  $\mathbf{B}$ :  $\mathbf{B}(:, n_B) \leftarrow \mathbf{a}_j$ 
33   Perform SVD on  $\mathbf{B}$ :  $[\mathbf{U}, \mathbf{\Sigma}, \mathbf{V}] = \text{svd}(\mathbf{B})$ 
34   Compute  $\eta \leftarrow \sigma_{n_B}^2$ , where  $\sigma_{n_B}^2$  is the  $n_B^{\text{th}}$  singular value of  $\mathbf{B}$ 
35    $\mathbf{B} \leftarrow \mathbf{U} \sqrt{\mathbf{\Sigma}^2 - \eta \mathbf{I}_{n_B}}$ 
36   return  $\mathbf{B}$ 
37 Function ApproximateRidgeScores( $\mathbf{B}, \mathbf{M}_{m \times t}, \|\mathbf{A}_{obs}\|_F^2$ ):
38   //  $\mathbf{M}$  contains any  $t$  columns from  $\mathbf{A}$ .
39   for  $i=1, \dots, t$  do
40      $\tau_i = (\mathbf{m}_i)^T (\mathbf{B}\mathbf{B}^T + \frac{\|\mathbf{A}_{obs}\|_F^2 - \|\mathbf{B}_k\|_F^2}{k} \mathbf{I})^\dagger (\mathbf{m}_i)$ 
41   end
42   return  $[\tau_1, \dots, \tau_t]$ 
```

The detailed implementation of the streaming ridge leverage score-based CSS is described in Algorithm 2. Regarding the input target rank k and basis size t , we set $k = t$ for simplicity in our implementation. Compared to the residual-based CSS explained in Section 2.2.1, this method prunes and updates the selected columns \mathbf{C} (Steps 12–27) and thus maintains a fixed RAM usage during the

CSS process. Therefore, we developed our randomized ID algorithm based on the streaming ridge leverage score-based CSS method.

3. Online randomized ID based on streaming CSS algorithm

The overall workflow of our online randomized ID approach is summarized in Fig. 1 and explained below. There are two major procedures in the framework: (1) perform a single-pass column subset selection (CSS) to identify the appropriate basis columns $\mathbf{A}_{\mathcal{J}}$ for approximation (Section 3.1), and (2) update the coefficient matrix \mathbf{P} whenever the basis columns change (Section 3.2). For the CSS procedure, we implement the streaming ridge leverage score-based CSS algorithm [21] to handle the streaming data. When a new data column arrives, the ridge leverage score of the new column is approximated using the currently selected columns, and the column subset is updated by random sampling based on the new leverage score.

The standard coefficient update procedure calculates the coefficients by solving a least squares problem:

$$\mathbf{P} = \arg \min_{\mathbf{X}} \|\mathbf{A}_{\mathcal{J}} \mathbf{X} - \mathbf{A}\|_F^2 \quad (21)$$

$$= (\mathbf{A}_{\mathcal{J}}^T \mathbf{A}_{\mathcal{J}})^{-1} \mathbf{A}_{\mathcal{J}}^T \mathbf{A} = \mathbf{A}_{\mathcal{J}}^{\dagger} \mathbf{A}. \quad (22)$$

However, the calculation of this \mathbf{P} requires full access to the data matrix \mathbf{A} , and hence requires a second pass over the data which we are trying to avoid. It is not possible to calculate the coefficients column-by-column during the first pass through the data since if a column \mathbf{a}_i is loaded, the index set \mathcal{J} may (eventually) contain indices j that are greater than i and so are not available at the time.

To address this issue, we apply random projections (cf. [12]) to compute a small matrix sketch of \mathbf{A} and store it in memory for the coefficient computation; this can be done in the same pass as the online CSS algorithm. Since the matrix sketch is used to compute the coefficient and an optimal coefficient is not guaranteed, we use four different methods (Algs. 4–7) to compute \mathbf{P} simultaneously. To determine the best coefficients, we implement an error estimator using the NA-Hutch++ algorithm [23] to approximate the Frobenius errors of the reconstructed data matrices (Section 3.3). The NA-Hutch++ is a single-pass stochastic algorithm that can reuse the matrix sketch obtained from random projection of \mathbf{A} for error estimation and thus can be easily accommodated in the online workflow. In addition, we apply a least squares method to estimate the gradient field, which is further used in the computation of the parameter matrix to ensure the gradient information of the physical field is well reconstructed (Section 3.4).

3.1. Streaming ridge leverage score based CSS using random projection

In Section 2.2.2, the ridge leverage score-based streaming CSS algorithm utilizes the frequent-directions sketch for approximating the ridge leverage score (Eq. (19)). Since the data matrix $\mathbf{A} \in \mathbb{R}^{m \times n}$ is assumed to have $m \gg n$, it is impractical to compute $\mathbf{B}\mathbf{B}^T \in \mathbb{R}^{m \times m}$ due to its large dimension. Instead, we perform random projection on each column to collect matrix sketch \mathbf{S} , which can also be used to compute the coefficient matrix and estimate the reconstruction in our workflow. Here, we define the ridge leverage score with respect to \mathbf{S} as

$$\tau_i = (\mathbf{\Omega} \mathbf{a}_i)^T \left(\mathbf{S} \mathbf{S}^T + \frac{\|\mathbf{A}_{obs}\|_F^2 - \|\mathbf{S}_k\|_F^2}{k} \mathbf{I} \right)^{\dagger} (\mathbf{\Omega} \mathbf{a}_i), \quad (23)$$

where $\mathbf{\Omega}$ is the Gaussian random matrix; \mathbf{A}_{obs} and $\mathbf{S} = \mathbf{\Omega} \mathbf{A}_{obs}$ are the observed data matrix and its sketch in the streaming setting, respectively; \mathbf{S}_k is the best rank- k approximation of \mathbf{S} . To adopt the random projection in the CSS process, we make the following modifications based on the original streaming CSS algorithm (Algorithm 2):

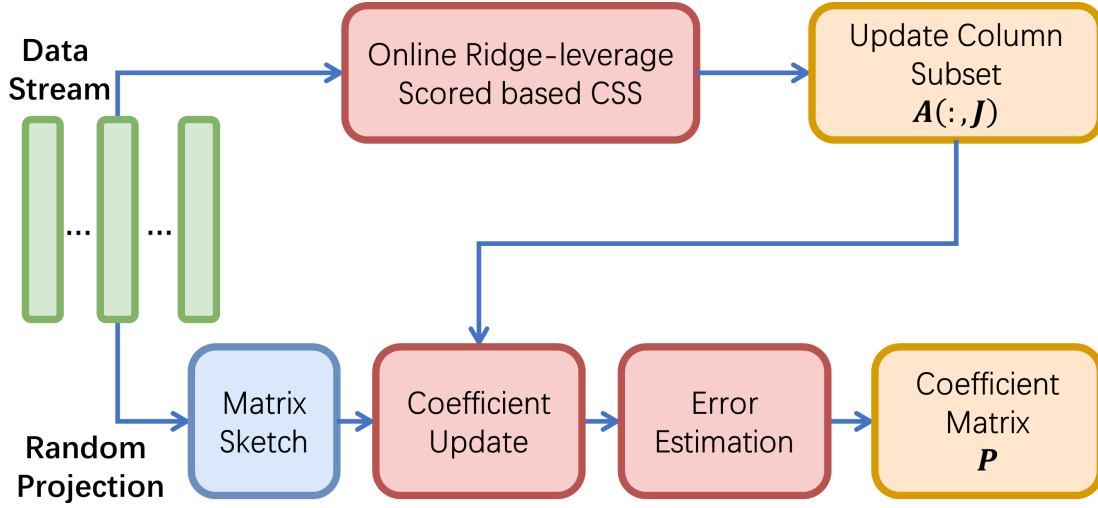


Figure 1: The workflow of our online randomized ID method.

- At the beginning of the CSS process, we generate the random projection matrix $\Omega_{\ell \times m}$ and then initialize the sketch matrix $\mathbf{S} = \mathbf{0}_{\ell \times n}$.
- The random projection is used to compute and collect the matrix sketch instead of frequent-directions.
- The ridge leverage scores for new columns in \mathbf{D} , $\tau^{\mathbf{D}}$, and previously selected columns \mathbf{C} , τ , with respect to the updated sketch \mathbf{S} are computed using Eq. (23).

The resulting pseudocode for the online randomized ID algorithm appears as Algorithm 3, where the detailed implementation of the modified CSS method is described in Steps 9–27. In Steps 28–32, we compute and update the coefficient matrix for the ID with the help of an error estimator. The detailed algorithms of Steps 29 and 30 will be explained in Sections 3.2 and 3.3.

Algorithm 3: Single-pass randomized ID algorithm

Input: Data matrix $\mathbf{A}_{m \times n}$, target rank k , basis size t , accuracy ϵ , success probability $(1 - \delta)$

Output: $\mathbf{A} \approx \mathbf{A}_{\mathcal{J}} \mathbf{P}$, where \mathcal{J} contains the indices of the selected columns

```
1 Choose  $\ell = k + p$ , where  $p$  is the oversampling parameter.
2 Generate Gaussian random matrix  $\mathbf{\Omega} = \text{randn}(\ell, m)$ 
3 Initialize the Frobenius norm of the observed data matrix as  $\|\mathbf{A}_{obs}\|_F^2 = 0$ 
4 Set  $count = 0$ ,  $\mathbf{C} = \mathbf{0}_{m \times t}$ ,  $\mathbf{D} = \mathbf{0}_{m \times t}$ 
5 Set  $\mathbf{S} = \mathbf{0}_{\ell \times t}$ ,  $\mathbf{S}\mathbf{S}^T = \mathbf{0}_{\ell \times \ell}$ 
6 Set the index set for the basis columns, the basis columns before the update, and the new
   columns as  $\mathcal{J}^C, \mathcal{J}_{prev}^C, \mathcal{J}^D \leftarrow \mathbf{0}_{t \times 1}$ 
7 Initialize  $[\tau_1^{old}, \dots, \tau_t^{old}] = 1$  for storing ridge leverage scores of  $\mathbf{C}$  with respect to previous read
   data columns.
8 for  $j = 1, \dots, n$  do
9   Read the next column  $j$  of  $\mathbf{A}$  into RAM, denoted by  $\mathbf{a}_j$ 
10  Compute and store sketched data  $\mathbf{s}_j = \mathbf{\Omega} \mathbf{a}_j$ ,  $\mathbf{S} \leftarrow [\mathbf{S}, \mathbf{s}_j]$ 
11   $\mathbf{S}\mathbf{S}^T \leftarrow \mathbf{S}\mathbf{S}^T + \mathbf{s}_j \mathbf{s}_j^T$ 
12  if  $count < t$  then
13     $\mathbf{d}_{count} = \mathbf{a}_j$ ,  $\mathcal{J}_{count}^D = j$ ,  $\|\mathbf{A}_{obs}\|_F^2 = \|\mathbf{A}_{obs}\|_F^2 + \|\mathbf{a}_j\|_2^2$ ,  $count \leftarrow count + 1$ 
14  else
15    // Follow the idea in [21] to compute ridge leverage score and prune column basis.
16    Update leverage scores of columns in  $\mathbf{C}$  as
17     $[\tau_1, \dots, \tau_t] = \min\{[\tau_1^{old}, \dots, \tau_t^{old}], \text{ApproximateRidgeScores\_Sketch}(\mathbf{S}\mathbf{S}^T, \mathbf{\Omega}, \mathbf{C}, \|\mathbf{A}_{obs}\|_F^2)\}$ 
18    Approximate leverage scores of new columns in  $\mathbf{D}$  as
19     $[\tau_1^D, \dots, \tau_t^D] = \text{ApproximateRidgeScores\_Sketch}(\mathbf{S}\mathbf{S}^T, \mathbf{\Omega}, \mathbf{D}, \|\mathbf{A}_{obs}\|_F^2)$ 
20    for  $i = 1, \dots, t$  do
21      if  $c_i \neq 0$  then
22        With probability  $(1 - \tau_i / \tau_i^{old})$ , set  $c_i = 0$ ,  $\tau_i^{old} = 1$  and  $\mathcal{J}_i^C = 0$ 
23        Otherwise set  $\tau_i^{old} = \tau_i$ 
24      end
25      if  $c_i = 0$  then
26        for  $r = 1, \dots, t$  do
27          With probability  $\frac{\tau_r^D c(k \log k + k \log(1/\delta)/\epsilon)}{t}$ , set  $c_i = \mathbf{d}_r$ ,  $\tau_i^{old} = \tau_r^D$  and
28           $\mathcal{J}_i^C = \mathcal{J}_r^D$ 
29        end
30      end
31    end
32  end
33  for  $q = 4, \dots, 7$  do
34     $\mathbf{P}_q = \text{CoefficientUpdate}(\mathcal{J}^C, \mathbf{\Omega} \mathbf{A}_{obs}, \mathcal{J}_{prev}^C, \text{algo} = q)$  ; // Via Algorithms 4--7,  $\mathcal{J}_{prev}^C$ 
35    is only required for  $q = 6, 7$ 
36     $e_q =$  approximation error estimated via single-pass Hutch++ (Algorithm 8)
37  end
38   $\mathbf{P} = \mathbf{P}_{q^*}$  where  $q^* = \arg \min_{q \in \{4, \dots, 7\}} e_q$ 
39   $\mathcal{J}_{prev}^C = \mathcal{J}^C$ ,  $count = 0$ 
40 end
41 end
42 Function ApproximateRidgeScores_Sketch( $\mathbf{S}\mathbf{S}^T$ ,  $\mathbf{\Omega}$ ,  $\mathbf{M}_{m \times t}$ ,  $\|\mathbf{A}_{obs}\|_F^2$ ):
43   //  $\mathbf{M}$  contains any  $t$  columns from  $\mathbf{A}$ .
44   for  $i = 1, \dots, t$  do
45      $\tau_i = (\mathbf{\Omega} \mathbf{m}_i)^T (\mathbf{S}\mathbf{S}^T + \frac{\|\mathbf{A}_{obs}\|_F^2 - \|\mathbf{S}_k\|_F^2}{k} \mathbf{I})^\dagger (\mathbf{\Omega} \mathbf{m}_i)$ 
46   end
47   return  $[\tau_1, \dots, \tau_t]$ 
```

3.2. Coefficient computation methods

Once we obtain the column basis via the streaming CSS algorithm, we can compute the coefficient matrix for the reconstruction of the original matrix. Due to the online setting, we need to quickly compute an accurate coefficient matrix for the observed data using the information stored in RAM. Since we use random projection to construct the data sketch in RAM, a standard approach is to solve the sketched version of Eq. (21) and obtain the coefficients. However, we lose the original data during the random projection and cannot guarantee an accurate reconstruction. To improve the reconstruction accuracy, it is essential to utilize the original data sufficiently in a streaming setting, and thus we implement four different methods (Algorithms 4–7) to simultaneously compute the coefficient matrices during the CSS process. We assume the column basis matrix $\mathbf{A}_{\mathcal{J}} \in \mathbb{R}^{m \times t}$ contains t columns, and the coefficient matrix $\mathbf{P} \in \mathbb{R}^{t \times n}$ is computed based on the observed data matrix $\mathbf{A}_{obs} = \mathbf{A}(:, 1 : n_{obs}) \in \mathbb{R}^{m \times n_{obs}}$, where n_{obs} is the number of the observed columns. In Algorithm 4, we first explain the standard approach to obtain the coefficients using the random projection sketch. Whenever the column basis is updated, we first get the new column basis sketch $\Omega \mathbf{A}_{\mathcal{J}}$ from the data matrix sketch $\Omega \mathbf{A}_{obs}$. Then, we solve the full sketching least squares problem to compute the updated coefficient matrix as

$$\mathbf{P} \approx \arg \min_{\mathbf{X}} \|\Omega \mathbf{A}_{\mathcal{J}} \mathbf{X} - \Omega \mathbf{A}_{obs}\|_F^2 = (\Omega \mathbf{A}_{\mathcal{J}})^\dagger (\Omega \mathbf{A}_{obs}). \quad (24)$$

Algorithm 4: Coefficient computation by directly solving fully sketched least squares problem

Input: Index set \mathcal{J} for the updated basis columns, current data matrix sketch $\Omega \mathbf{A}_{obs}$

- 1 Solve the least squares problem $\mathbf{P} = \arg \min_{\mathbf{X}} \|\Omega \mathbf{A}_{\mathcal{J}} \mathbf{X} - \Omega \mathbf{A}_{obs}\|_F^2$

Output: \mathbf{P}

In addition to $\Omega \mathbf{A}_{obs}$, the column basis matrix $\mathbf{A}_{\mathcal{J}}$ containing the original data is also stored in RAM and can be used for the coefficient computation. To take advantage of these data, in Algorithm 5, we compute the coefficient matrix by applying the pseudoinverse of the selected column basis on the data matrix (Eq. (22)). In particular, we use both original and sketched column bases to approximate the pseudoinverse $\mathbf{A}_{\mathcal{J}}^\dagger$, motivated by similar approaches in [31, 32]. Whenever the column basis is updated, we first use the column basis to compute

$$\mathbf{G} = \mathbf{A}_{\mathcal{J}}^T \mathbf{A}_{\mathcal{J}}. \quad (25)$$

Then, we use the sketched data matrix to approximate

$$\mathbf{A}_{\mathcal{J}}^T \mathbf{A} \approx (\Omega \mathbf{A}_{\mathcal{J}})^T (\Omega \mathbf{A}_{obs}) =: \mathbf{Y}. \quad (26)$$

The coefficient matrix is then obtained as $\mathbf{P} \approx \mathbf{G}^{-1} \mathbf{Y}$.

Algorithm 5: Coefficient computation based on partial sketching of new data column

Input: Index set \mathcal{J} for the updated basis columns, current data matrix sketch $\Omega \mathbf{A}_{obs}$

- 1 Compute and store $\mathbf{G} = \mathbf{A}_{\mathcal{J}}^T \mathbf{A}_{\mathcal{J}}$, $\mathbf{Y} = (\Omega \mathbf{A}_{\mathcal{J}})^T (\Omega \mathbf{A}_{obs})$; *// Approximate $\mathbf{Y} = \mathbf{A}_{\mathcal{J}}^T \mathbf{A}_{obs}$ using sketched data.*
- 2 $\mathbf{P} = \mathbf{G}^{-1} \mathbf{Y}$

Output: \mathbf{P}

In the online CSS process, the column bases are only partially pruned and updated with newly selected columns rather than entirely replaced with a new set of columns. Therefore, it is inefficient to solve the fully sketched problem repeatedly as in Algorithm 4 to get new coefficients. Instead, we

can reuse and improve the reconstruction based on the results from the previous column basis update. In Algorithm 6, we reuse the unchanged basis and update the coefficients based on the values derived using the old basis. In detail, whenever the column basis is updated, we first determine the indices of the unchanged column basis \mathcal{I}_{uc} in the previous index set \mathcal{J}_{prev} . In the previous coefficient matrix, we zero out the rows corresponding to the replaced columns,

$$\mathbf{P}_{prev}(i, :) \leftarrow \begin{cases} \mathbf{P}_{prev}(i, :), & i \in \mathcal{I}_{uc} \\ \mathbf{0}, & \text{otherwise} \end{cases} \quad \text{for } i = 1, \dots, t. \quad (27)$$

We then compute the approximation residual using the unchanged basis as

$$\mathbf{r}_A = \Omega \mathbf{A} - \Omega \mathbf{A}_{\mathcal{J}} \mathbf{P}_{prev}. \quad (28)$$

Then, we use the new column basis to approximate the residual and obtain the new coefficient matrix as

$$\delta \mathbf{P} = \arg \min_{\mathbf{X}} \|\Omega \mathbf{A}_{\mathcal{J}} \mathbf{X} - \mathbf{r}_A\|_F^2, \quad (29)$$

$$\mathbf{P} = \mathbf{P}_{prev} + \delta \mathbf{P}. \quad (30)$$

Algorithm 6: Coefficient computation based on the residual of fully sketched least squares problem

Input: Index sets \mathcal{J} , \mathcal{J}_{prev} for the updated and previous basis columns, respectively, the previous coefficient matrix \mathbf{P}_{prev} , current data matrix sketch $\Omega \mathbf{A}_{obs}$

- 1 Determine the unchanged column indices in \mathcal{J}_{prev} as \mathcal{I}_{uc} ,
- 2 Update \mathbf{P}_{prev} with \mathcal{I}_{uc} using Eq. (27).
- 3 Compute approximation residual $\mathbf{r}_A = \Omega \mathbf{A}_{obs} - \Omega \mathbf{A}_{\mathcal{J}} \mathbf{P}_{prev}$
- 4 Solve the least squares problem $\delta \mathbf{P} = \arg \min_{\mathbf{X}} \|\Omega \mathbf{A}_{\mathcal{J}} \mathbf{X} - \Omega \mathbf{A}_{obs}\|_F^2$
- 5 $\mathbf{P} = \mathbf{P}_{prev} + \delta \mathbf{P}$

Output: \mathbf{P}

In Algorithm 7, we utilize the QR decomposition of the selected column basis to compute the coefficients instead of directly solving the fully sketched least squares problem. Whenever the column basis is updated, we compute the QR on the updated column basis sketch

$$\Omega \mathbf{A}_{\mathcal{J}} = \mathbf{Q} \mathbf{R}. \quad (31)$$

We then compute the transformation matrix from new to old column basis and update the old coefficient matrix as

$$\mathbf{T} = \mathbf{R}^{-1} \mathbf{Q}^{-1} \Omega \mathbf{A}_{\mathcal{J}_{prev}}, \mathbf{P} = \mathbf{T} \mathbf{P}_{prev}. \quad (32)$$

Algorithm 7: Coefficient computation based on QR decomposition update

Input: Index sets \mathcal{J} , \mathcal{J}_{prev} for the updated and previous basis columns, respectively, the previous coefficient matrix \mathbf{P}_{prev} , current data matrix sketch $\Omega \mathbf{A}_{obs}$

- 1 Compute $\mathbf{Q}, \mathbf{R} = qr(\Omega \mathbf{A}_{\mathcal{J}})$
- 2 Compute the transformation matrix from new to old column basis as $\mathbf{T} = \mathbf{R}^{-1} \mathbf{Q}^{-1} \Omega \mathbf{A}_{\mathcal{J}_{prev}}$
- 3 Update the coefficient matrix $\mathbf{P} = \mathbf{T} \mathbf{P}_{prev}$

Output: \mathbf{P}

3.3. Single-pass Hutch++ for error estimation

We seek an *a posteriori* estimate of the reconstruction error because it is inherently useful and because we can apply all four algorithms presented in Section 3.2 simultaneously (using the same sketched data) and use the error estimate to select whichever method is best. Given our emphasis on online compression, we adopt the NA-Hutch++ trace estimation algorithm in [23] as it requires only a single pass over the data to estimate the Frobenius norm error $\|\mathbf{E}\|_F = \|\mathbf{A} - \mathbf{A}_{\mathcal{J}}\mathbf{P}\|_F$. In more detail, the NA-Hutch++ algorithm builds on the well-known Hutchinson’s stochastic trace estimator [33]. Let $\mathbf{B} = \mathbf{E}\mathbf{E}^T \in \mathbb{R}^{m \times m}$ be a square matrix and $\mathbf{\Omega} = [\boldsymbol{\omega}_1, \dots, \boldsymbol{\omega}_\ell]^T \in \mathbb{R}^{\ell \times m}$ a matrix containing i.i.d. random variables with mean 0 and variance 1. For each $\boldsymbol{\omega}_j \in \mathbb{R}^m$, the expectation of $\boldsymbol{\omega}_j^T \mathbf{B} \boldsymbol{\omega}_j$ equals the trace of \mathbf{B} . The Hutchinson estimator approximates $\|\mathbf{E}\|_F^2 = \text{tr}(\mathbf{B})$ as

$$\text{tr}(\mathbf{B}) \approx \frac{1}{\ell} \sum_{j=1}^{\ell} \boldsymbol{\omega}_j^T \mathbf{B} \boldsymbol{\omega}_j = \frac{1}{\ell} \text{tr}(\mathbf{\Omega} \mathbf{B} \mathbf{\Omega}^T), \quad (33)$$

where ℓ represents the number of “matrix-vector” multiplication queries. This amounts to a Monte Carlo approach, so accuracy improves very slowly as ℓ increases, which has motivated modern improvements, such as Hutch++ [23], which use low-rank approximation as control variates to improve the estimate, though these methods are not one-pass. Instead, we turn to the NA-Hutch++ algorithm which is one-pass and has nearly the same theoretical guarantees as Hutch++ (proved in [23]), leading to more accurate trace estimation as compared to Eq. (33). Instead of querying once with a single random matrix $\mathbf{\Omega}$, the NA-Hutch++ draws three sub-Gaussian random matrices $\mathbf{H} \in \mathbb{R}^{c_1 \ell \times m}$, $\mathbf{R} \in \mathbb{R}^{c_2 \ell \times m}$ and $\mathbf{G} \in \mathbb{R}^{c_3 \ell \times m}$, where $c_1 \ell$, $c_2 \ell$, and $c_3 \ell$ are all integers satisfying $(c_1 + c_2 + c_3) = 1$. Then, given $c_2 > c_1$ and $\ell = \mathcal{O}(k \log(1/\delta))$, with probability $1 - \delta$, an approximation of \mathbf{B} can be constructed as

$$\tilde{\mathbf{B}} = (\mathbf{R}\mathbf{B})^T (\mathbf{H}\mathbf{B}\mathbf{R}^T)^\dagger (\mathbf{H}\mathbf{B}), \quad (34)$$

which satisfies $\|\mathbf{B} - \tilde{\mathbf{B}}\|_F \leq 2\|\mathbf{B} - \mathbf{B}_k\|_F$ [34], and thus can be used to approximate $\text{tr}(\mathbf{B})$. By using the cyclic property of the trace, NA-Hutch++ computes $\text{tr}(\tilde{\mathbf{B}})$ efficiently without explicitly constructing $\tilde{\mathbf{B}}$ as

$$\begin{aligned} \text{tr}(\mathbf{B}) \approx \text{tr}(\tilde{\mathbf{B}}) &= \text{tr}((\mathbf{H}\mathbf{B}\mathbf{R}^T)^\dagger (\mathbf{H}\mathbf{B})(\mathbf{R}\mathbf{B})^T) \\ &+ \frac{1}{c_3 \ell} [\text{tr}(\mathbf{G}\mathbf{B}\mathbf{G}^T) - \text{tr}(\mathbf{G}\tilde{\mathbf{B}}\mathbf{G}^T)], \end{aligned} \quad (35)$$

where the terms in the second row are approximated using the Hutchinson estimator with the random vectors in \mathbf{G} . By substituting Eq. (35) with $\mathbf{B} = \mathbf{E}\mathbf{E}^T$ and have

$$\begin{aligned} \text{tr}(\mathbf{E}\mathbf{E}^T) &= \text{tr}((\mathbf{H}\mathbf{E}(\mathbf{R}\mathbf{E})^T)^\dagger (\mathbf{H}\mathbf{E}\mathbf{E}^T)(\mathbf{R}\mathbf{E}\mathbf{E}^T)^T) \\ &+ \frac{1}{c_3 \ell} [\text{tr}(\mathbf{G}\mathbf{E}(\mathbf{G}\mathbf{E})^T) - \text{tr}(\mathbf{G}\mathbf{E}(\mathbf{R}\mathbf{E})^T (\mathbf{H}\mathbf{E}(\mathbf{R}\mathbf{E})^T)^\dagger (\mathbf{H}\mathbf{E})(\mathbf{G}\mathbf{E})^T)]. \end{aligned} \quad (36)$$

Note that we can sample the row of random project matrix $\mathbf{\Omega}$ to obtain random matrices \mathbf{R} , \mathbf{H} and \mathbf{G} without duplicated rows. Accordingly, we can also obtain three query matrices $\mathbf{R}\mathbf{E} = \mathbf{R}(\mathbf{A} - \mathbf{A}_{\mathcal{J}}\mathbf{P})$, $\mathbf{H}\mathbf{E} = \mathbf{H}(\mathbf{A} - \mathbf{A}_{\mathcal{J}}\mathbf{P})$ and $\mathbf{G}\mathbf{E} = \mathbf{G}(\mathbf{A} - \mathbf{A}_{\mathcal{J}}\mathbf{P})$ by reusing the corresponding rows of the sketched data $\mathbf{\Omega}(\mathbf{A} - \mathbf{A}_{\mathcal{J}}\mathbf{P})$, and thus the query process can be easily accommodated in the online randomized ID pipeline (Step 30 in Algorithm 3). In addition, the trace possesses the following linearity property

$$\text{tr}(\mathbf{E}\mathbf{E}^T) = \text{tr} \left(\sum_{j=1}^n \mathbf{e}_j \mathbf{e}_j^T \right) = \sum_{j=1}^n \text{tr}(\mathbf{e}_j \mathbf{e}_j^T), \quad (37)$$

and thus $\text{tr}(\mathbf{E}\mathbf{E}^T)$ can be incrementally evaluated in a single pass by computing the contribution from each column of \mathbf{E} . In particular, we apply Eq. (36) to each column \mathbf{e}_j to compute $\text{tr}(\mathbf{e}_j\mathbf{e}_j^T)$ and incrementally update $\text{tr}(\mathbf{E}\mathbf{E}^T)$ until all data columns are observed. The detailed implementation of each update of the incremental error estimator is shown in Algorithm 8.

Algorithm 8: NA-Hutch++ [23] for the incremental error estimation of online randomized ID

Input: New data column \mathbf{a}_j , selected columns $\mathbf{A}_{\mathcal{J}}$, parameter matrix \mathbf{P} , random matrix $\mathbf{\Omega}_{\ell \times m}$, current trace $\text{tr}(\mathbf{E}\mathbf{E}^T)$, constants c_1, c_2 , and c_3 where $c_1 < c_2$ and $c_1 + c_2 + c_3 = 1$, and $c_1\ell, c_2\ell, c_3\ell \in \mathbb{N}$,

- 1 Compute the error of the new data column $\mathbf{e}_j = \mathbf{a}_j - \mathbf{A}_{\mathcal{J}}\mathbf{P}(:, j)$
 - 2 Compute query matrix $\mathbf{E}_q = \mathbf{e}_j(\mathbf{\Omega}\mathbf{e}_j)^T$
 - 3 Sampling from the row of $\mathbf{\Omega}$ and obtain three index sets $\mathcal{I}_H, \mathcal{I}_R, \mathcal{I}_G$ with sizes $c_1\ell, c_2\ell, c_3\ell$.
 - 4 Set sample matrices $\mathbf{H} = \mathbf{\Omega}(\mathcal{I}_H, :)$, $\mathbf{R} = \mathbf{\Omega}(\mathcal{I}_R, :)$, $\mathbf{G} = \mathbf{\Omega}(\mathcal{I}_G, :)$
 - 5 Compute $\mathbf{Z} = \mathbf{e}_j(\mathbf{R}\mathbf{e}_j)^T = \mathbf{E}_q(:, \mathcal{I}_R)$, $\mathbf{W} = \mathbf{e}_j(\mathbf{H}\mathbf{e}_j)^T = \mathbf{E}_q(:, \mathcal{I}_H)$ and $\mathbf{G}\mathbf{e}_j(\mathbf{G}\mathbf{e}_j)^T = \mathbf{E}_q(:, \mathcal{I}_G)\mathbf{E}_q(:, \mathcal{I}_G)^T$
 - 6 Compute new trace contribution from \mathbf{e}_j as $\text{tr}(\mathbf{e}_j\mathbf{e}_j^T) = \text{tr}((\mathbf{H}\mathbf{Z}^T)^\dagger(\mathbf{W}^T\mathbf{Z})) + \frac{1}{c_3\ell}[\text{tr}(\mathbf{G}\mathbf{e}_j(\mathbf{G}\mathbf{e}_j)^T) - \text{tr}(\mathbf{G}\mathbf{Z}(\mathbf{H}\mathbf{Z}^T)^\dagger\mathbf{W}^T\mathbf{G}^T)]$
 - 7 $\text{tr}(\mathbf{E}\mathbf{E}^T) \leftarrow \text{tr}(\mathbf{E}\mathbf{E}^T) + \text{tr}(\mathbf{e}_j\mathbf{e}_j^T)$
- Output:** $\text{tr}(\mathbf{E}\mathbf{E}^T)$
-

3.4. Enhancing the randomized ID with estimated gradient information

In many scientific applications, the quantities of interest (QoIs) are obtained by postprocessing the solution to the governing equations. For instance, in computational fluid dynamics, the vorticity field is computed based on the gradient of the velocity field. When only the solution data is compressed, however, the quality of the QoIs generated from the reconstructed data may be poor. To address this issue, we consider the scenario where the QoI is the gradient of the solution, and present a modification of the online randomized ID approach that incorporates the gradient information in the compression process. In Section 4, we show that for a fixed basis size, the modified ID approach leads to considerably more accurate solution gradients at the expense of a slight decrease in the accuracy of the reconstructed solution.

To account for the gradient information in our compression framework, we first apply a least squares method to estimate the gradient of the reconstructed data assuming a graph structure for the underlying mesh; such gradient estimates are often referred to as *simplex gradients* [35]. Let $\mathcal{G} = (\mathcal{V}, \mathcal{E})$ be a finite graph, where \mathcal{V} and \mathcal{E} denote the vertices and edges of the graph, respectively; $\mathbf{x}(\mathcal{V})$ denotes the d -dimensional spatial coordinates of the vertices; $F(\mathcal{V})$ denotes the physical field of interest defined on this graph, i.e., the data stored in \mathbf{A} . For each vertex $v_i \in \mathcal{V}$, we define its 1-ring neighborhood $\mathcal{N}_i = \{v_j\}_{j=1}^{n_i}$ such that each vertex v_j is directly connected to v_i and n_i is the number of the neighboring vertices. We denote $\mathcal{N}_i(j)$ as the j^{th} vertex in the 1-ring neighborhood. In the 1-ring neighborhood of each node v_i , we have

$$F(v_j) - F(v_i) \approx \nabla F \cdot (\mathbf{x}(v_j) - \mathbf{x}(v_i)), \quad j = 0, \dots, n_i. \quad (38)$$

By collecting all the $\mathbf{x}(v_j) - \mathbf{x}(v_i)$ in a matrix \mathbf{K}_i and $F(v_j) - F(v_i)$ in a vector \mathbf{f}_i , we have

$$\mathbf{K}_i = \begin{bmatrix} \mathbf{x}(v_1) - \mathbf{x}(v_i) \\ \vdots \\ \mathbf{x}(v_j) - \mathbf{x}(v_i) \\ \vdots \\ \mathbf{x}(v_{n_i}) - \mathbf{x}(v_i) \end{bmatrix}, \quad \mathbf{f}_i = \begin{bmatrix} F(v_1) - F(v_i) \\ \vdots \\ F(v_j) - F(v_i) \\ \vdots \\ F(v_{n_i}) - F(v_i) \end{bmatrix}. \quad (39)$$

We rewrite Eq. (38) as the linear system

$$\mathbf{K}_i \nabla F(v_i) = \mathbf{f}_i, \quad (40)$$

which is usually overdetermined ($n_i > d$) for the commonly used meshes such as the 2D or 3D structured grids. The least squares approximation of $\nabla F(v_i)$ can be obtained from

$$\nabla F(v_i) = \mathbf{K}_i^\dagger \mathbf{f}_i. \quad (41)$$

By computing and assembling the local matrix \mathbf{K}_i^\dagger of each vertex on the entire graph, we can build the global gradient estimation operator \mathbf{G} as

$$\mathbf{G} = \begin{bmatrix} \mathbf{G}^1 \\ \vdots \\ \mathbf{G}^p \\ \vdots \\ \mathbf{G}^d \end{bmatrix}, \quad (42)$$

where \mathbf{G}^p is the gradient estimation matrix of the p^{th} spatial dimension and is defined as

$$\mathbf{G}^p(i, j) \leftarrow \begin{cases} \mathbf{K}_i^\dagger(p, k), & v_j = \mathcal{N}_i(k) \\ -\sum_{k=1}^{n_i} \mathbf{K}_i^\dagger(p, k), & v_j = v_i \\ \mathbf{0}, & \text{otherwise} \end{cases} \quad \text{for } j = 1, \dots, m. \quad (43)$$

Note that \mathbf{G} can be stored as a sparse matrix since each row has only $n_i + 1$ non-zero elements. It can be used in both CSS and coefficient computation procedures for gradient estimation and improving the reconstruction of the gradient field. During the CSS procedure, the gradient information helps to select a better column basis accounting for the gradient information. In more detail, in Step 10 of the CSS algorithm (Algorithm 3), we obtain the estimated gradient $\mathbf{G}\mathbf{a}_j$ for each new data column \mathbf{a}_j , and concatenate the estimated gradient vector with \mathbf{a}_j to approximate the ridge leverage scores for column selection. The gradient estimate is discarded after the ridge leverage score is computed to reduce memory usage. The ID coefficient matrix can then be obtained by the augmented optimization problem

$$\mathbf{P}(\lambda) = \arg \min_{\mathbf{X}} \left(\|\mathbf{A}_{\mathcal{J}} \mathbf{X} - \mathbf{A}\|_F^2 + \lambda \sum_{p=1}^d \|\mathbf{G}^p \mathbf{A}_{\mathcal{J}} \mathbf{X} - \mathbf{G}^p \mathbf{A}\|_F^2 \right), \quad (44)$$

where λ is a regularization parameter. In our implementation, we solve the full sketching least squares problem of Eq. (44) to approximate the coefficient matrix as

$$\mathbf{P}(\lambda) \approx \arg \min_{\mathbf{X}} \left(\|\boldsymbol{\Omega}(\mathbf{A}_{\mathcal{J}} \mathbf{X} - \mathbf{A})\|_F^2 + \lambda \sum_{p=1}^d \|\boldsymbol{\Omega}(\mathbf{G}^p \mathbf{A}_{\mathcal{J}} \mathbf{X} - \mathbf{G}^p \mathbf{A})\|_F^2 \right), \quad (45)$$

Moreover, to determine the best λ , we follow the generalized cross-validation (GCV) method [36] to minimize the GCV function

$$\text{GCV}(\lambda) = \frac{\|(\mathbf{I} - \mathbf{C}^\natural(\lambda))\mathbf{A}\|_F^2}{\left(\text{tr}(\mathbf{I} - \mathbf{C}^\natural(\lambda))\right)^2}. \quad (46)$$

where $\mathbf{C}^\natural(\lambda)$ is defined as

$$\mathbf{C}^\natural(\lambda) = \mathbf{A}_{\mathcal{J}} \left(\mathbf{A}_{\mathcal{J}}^T \mathbf{A}_{\mathcal{J}} + \lambda \sum_{p=1}^d (\mathbf{G}^p \mathbf{A}_{\mathcal{J}})^T \mathbf{G}^p \mathbf{A}_{\mathcal{J}} \right)^{-1} \left(\mathbf{A}_{\mathcal{J}} + \lambda \sum_{p=1}^d (\mathbf{G}^p)^T \mathbf{G}^p \mathbf{A}_{\mathcal{J}} \right)^T. \quad (47)$$

such that it satisfies

$$\mathbf{P}(\lambda) = \mathbf{C}^\natural(\lambda)\mathbf{A}, \quad (48)$$

In particular, we use the random projection matrix $\mathbf{\Omega}$ and the sketched data $\mathbf{\Omega}\mathbf{A}$ to approximate the GCV function in a single pass as

$$\text{GCV}(\lambda) \approx \frac{\|(\mathbf{I} - \mathbf{C}^\natural_\Omega(\lambda))\mathbf{\Omega}\mathbf{A}\|_F^2}{\left(\text{tr}(\mathbf{I} - \mathbf{C}^\natural_\Omega(\lambda))\right)^2}, \quad (49)$$

where

$$\mathbf{C}^\natural_\Omega(\lambda) = \mathbf{\Omega}\mathbf{A}_\mathcal{J} \left((\mathbf{\Omega}\mathbf{A}_\mathcal{J})^T (\mathbf{\Omega}\mathbf{A}_\mathcal{J}) + \lambda \sum_{p=1}^d (\mathbf{\Omega}\mathbf{G}^p \mathbf{A}_\mathcal{J})^T \mathbf{\Omega}\mathbf{G}^p \mathbf{A}_\mathcal{J} \right)^{-1} \left(\mathbf{\Omega}^T \mathbf{\Omega}\mathbf{A}_\mathcal{J} + \lambda \sum_{p=1}^d (\mathbf{\Omega}\mathbf{G}^p)^T \mathbf{\Omega}\mathbf{G}^p \mathbf{A}_\mathcal{J} \right)^T. \quad (50)$$

By minimizing the estimated GCV function, we obtain the best λ .

4. Numerical experiments

The online randomized ID algorithms proposed in this work are tested on the following three datasets:

- The JHU turbulence flow data from the direct numerical simulation of a turbulent channel flow in a domain of size $8\pi \times 2 \times 3\pi$, using $2048 \times 512 \times 1536$ nodes [24, 25, 26]. The dataset contains 4,000 frames of data after the simulation reaches a statistically stationary state. The frictional Reynolds number is $Re_\tau \approx 1000$.
- The ignition dataset consists of species concentration in a jet diffusion simulation computed on a 50×50 grid over 450 time steps.
- The NSTX Gas Puff Image (GPI) data [28, 29] consists of 2D time-series data on 80×64 grid in 300,000 time steps.

In our experiments, we measure the relative Frobenius error and wall-clock runtime of our algorithm and benchmark against the offline SVD and two-pass ID. We will demonstrate the effectiveness of our approach by comparing it with other approaches in terms of both CSS and coefficient calculation steps.

4.1. Turbulent channel flow

We first test our algorithm on the dataset extracted from the turbulence channel flow simulation result of 4000 frames [24, 25, 26]. We collect the x -direction velocity field (u_x) on 64×64 , 128×128 and 256×256 grids at the $y = 1$ plane through time. Therefore, we obtain three data matrices of 4000 snapshots with 4096, 16,384, and 65,536 grid points per snapshot, respectively. We set $\delta = 0.05$ and $\epsilon = 0.5$ in Algorithm 2 to perform CSS. The reconstruction result of different time steps with target rank $k = 50$ is shown in Figs. 2–4. We find that most turbulence features are well captured in the reconstruction result. However, we also observe ripple shapes that appear in some reconstruction images (Step 220 in Fig. 2, Step 920 in Fig. 3) causing a larger reconstruction error.

To evaluate the performance of our approach, we measure the effect of the target rank k on the relative error (measured in terms of the Frobenius norm) of different coefficient computation algorithms as shown in Table 1. We select the truncated SVD method and the single-pass randomized

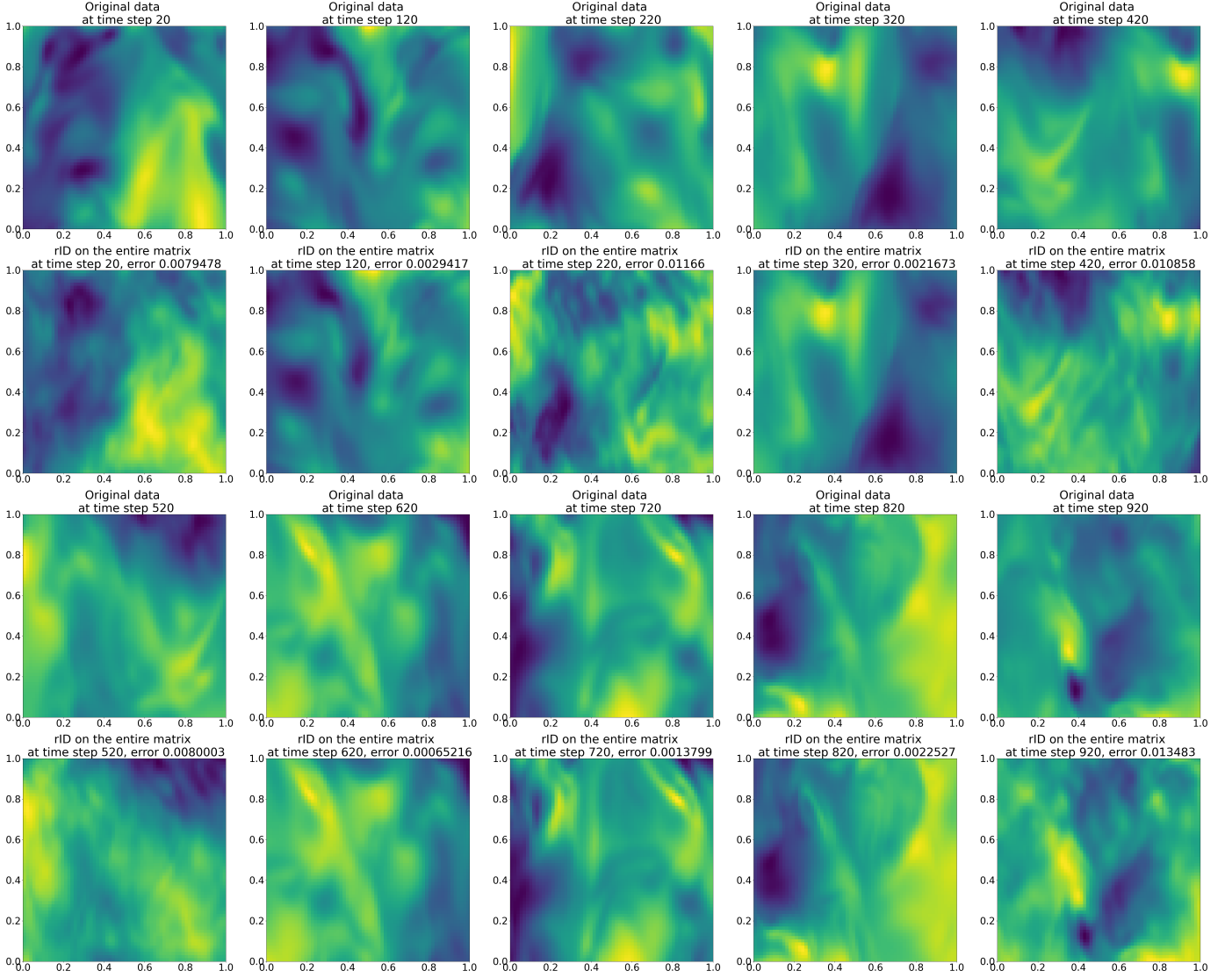


Figure 2: Rank $k = 50$ reconstruction of turbulence flow data over a 64×64 grid at different time steps. For each two rows, the top one represents the original data while the bottom one represents the reconstruction data.

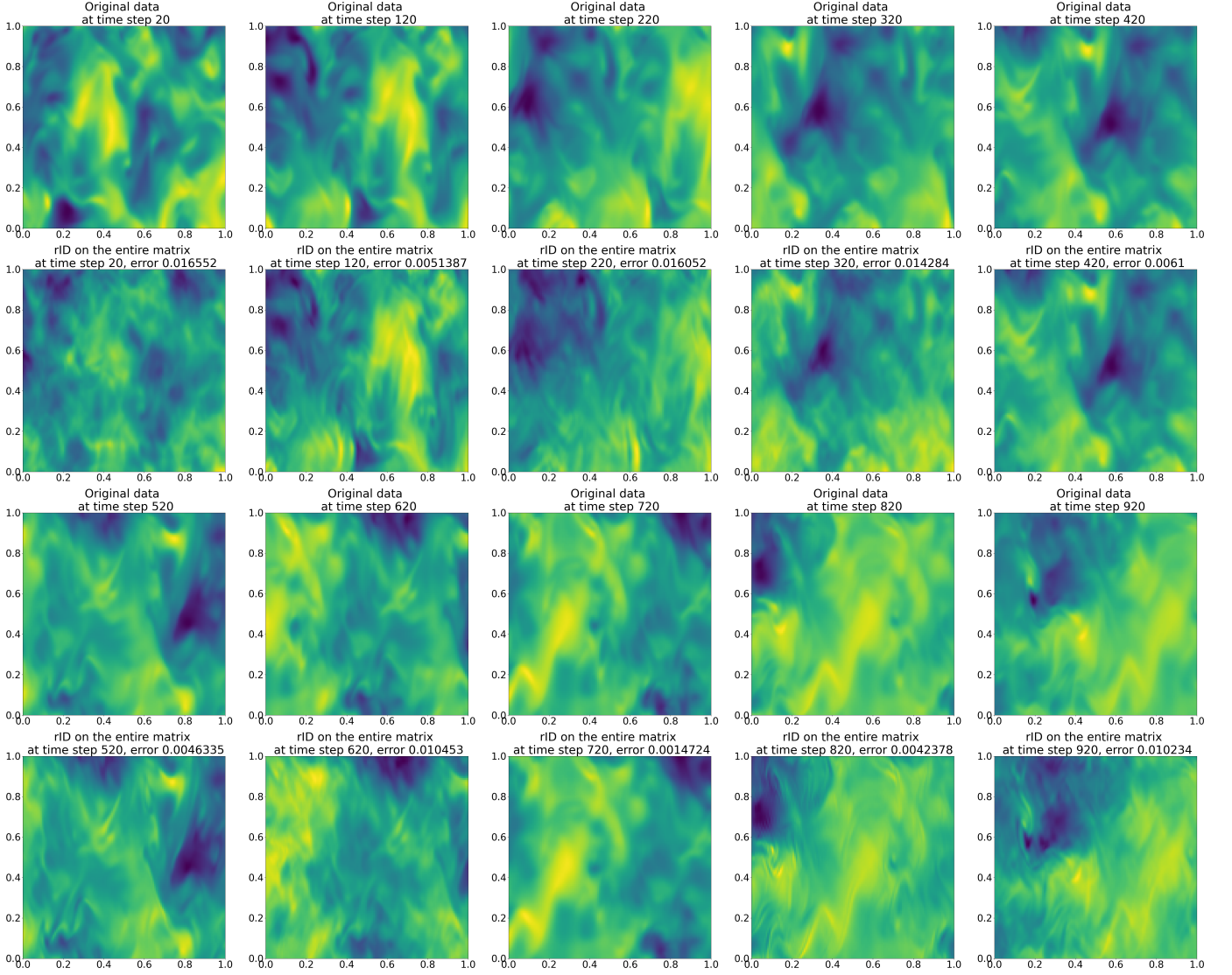


Figure 3: Rank $k = 50$ reconstruction of turbulence flow data over a 128×128 grid at different time steps. For each two rows, the top one represents the original data while the bottom one represents the reconstruction data.

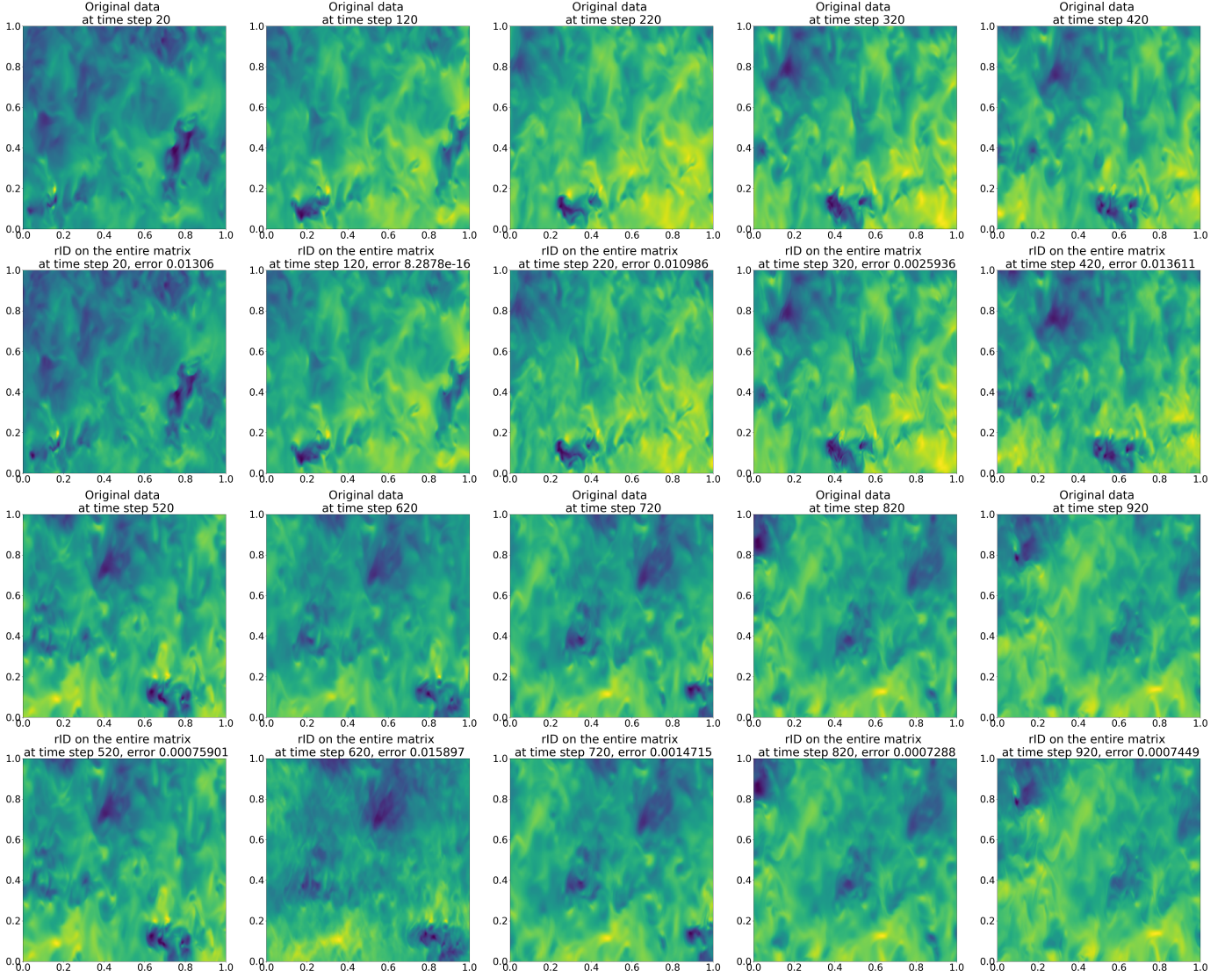


Figure 4: Rank $k = 50$ reconstruction of turbulence flow data over a 256×256 grid at different time steps. For each two rows, the top one represents the original data while the bottom one represents the reconstruction data.

SVD [13] using different target ranks as the benchmarks for comparison. For the residual-based CSS (Algorithm 1), to ensure its memory usage of column basis is the same as other approaches, we only expand its column subset until k columns are selected and any new column will not be added to the subset. The same treatment is also used in the remaining experiments of this paper. For each case, we also record the relative error estimated using the single-pass Hutch++ method. As expected, we find that the reconstruction accuracy keeps improving along with the target rank. Given the same rank, we use bold fonts for the exact and estimated relative Frobenius error with the least value. We find that the accuracy difference between the coefficients obtained from the four strategies of Section 3.2 is very small in this experiment. In addition, the single-pass Hutch++ method accurately estimates the relative Frobenius error and determines the coefficient matrix with the least reconstruction error.

To isolate just the impact of the ridge leverage score-based CSS algorithm, we first compare it with other CSS methods based on CPQR, residual norm (Algorithm 1), and standard leverage score sampling [37] in a two-pass setting. In these other approaches, we first obtain the indices of the selected columns \mathcal{J} and then compute the coefficient matrix by directly solving Eq. (21) without sketching. The ridge leverage score-based CSS performs slightly worse than the standard leverage score method, which is reasonable since the score is approximated in a streaming setting. It also performs better than the residual-based CSS but the CPQR outperforms all the other approaches. In Table 1, we then compare the ridge leverage score-based CSS (Algorithm 2) with the residual-based CSS (Algorithm 1) in an online setting where the coefficient matrix is computed simultaneously with CSS using Algs. 4–7. In most cases, our choice of CSS approach obtains better reconstruction accuracy than the residual-based CSS method.

For the turbulence channel flow dataset, it is also important to maintain an accurate reconstruction of vorticity. Since the computation of vorticity utilizes the gradient of the velocity, we need to account for the gradient reconstruction and thus compared four testing cases: (1) no gradient estimation; (2) using gradient estimation in coefficient computation; (3) using gradient estimation in CSS; and (4) using gradient estimation in both CSS and coefficient computation. In Table 2, we summarize the reconstruction error of both the velocity and vorticity fields. We find that the vorticity accuracy increases when the gradient information is used in both CSS and coefficient computation procedures. Regarding the velocity reconstruction, when the gradient information is only used in computing the coefficient matrix, the velocity accuracy slightly decreases as a tradeoff since the optimization (Eq. (44)) also accounts for the minimization of the gradient field error. However, the vorticity reconstruction becomes more accurate when the gradient information is used. In Fig. 5, we plot and compare the original vorticity (1st row) with the reconstructed vorticity field using the aforementioned four cases at different time steps.

In Table 3, we compare the runtime of our online randomized ID method with the offline ID via CPQR and the online randomized SVD [13]. We find that the computational time of our randomized ID method decreases along with the target rank and becomes stable when the rank size is around 50. The offline ID method is faster compared to the two online algorithms but our method achieves comparable runtime when the target rank is 100. Compared to the single-pass randomized SVD method, our method shows an advantage when the target rank is higher and we can also achieve comparable reconstruction accuracy, as shown in Table 1. In addition, our implementation is optimized for pass efficiency rather than computational efficiency, and thus the runtime does not show an advantage over the offline ID via CPQR for a small dataset.

Table 1: The relative error of randomized ID with different coefficient computation algorithms and different numbers of new columns. The estimated error using single-pass Hutch++ is included in the bracket. The testing is performed on the turbulence channel flow dataset

Dataset	# passes	Column selection	Coeff. update	Target rank					
				5	10	20	40	50	100
Channel flow $64 \times 64 \times 1000$	2	Truncated SVD	Randomized SVD	1.61%	1.17%	0.78%	0.41%	0.31%	0.11%
	1			1.71%	1.40%	1.21%	0.72%	0.58%	0.23%
	k	CPQR	Least squares (Eq. (22))	2.51%	2.30%	1.58%	1.20%	0.97%	0.47%
	2	Leverage score	Least squares (Eq. (22))	3.17%	2.84%	1.86%	1.94%	1.22%	1.15%
	2	Residual-based (Algorithm 1)	Least squares (Eq. (22))	3.47%	3.05%	2.75%	2.61%	1.39%	1.22%
	2	Ridge leverage score-based (Algorithm 3)	Least squares (Eq. (22))	3.25%	3.01%	2.12%	2.04%	1.35%	1.21%
	1	Residual-based (Algorithm 1)	Algorithm 4	4.45%(4.67%)	3.35%(3.97%)	3.78%(4.25%)	3.62%(4.35%)	2.75%(3.94%)	2.29%(2.82%)
	1	Residual-based (Algorithm 1)	Algorithm 5	4.15%(4.34%)	3.17%(3.52%)	4.75%(4.96%)	5.73%(6.34%)	6.91%(7.83%)	4.73%(5.02%)
	1	Residual-based (Algorithm 1)	Algorithm 6	4.69%(4.82%)	4.52%(4.71%)	4.18%(4.53%)	5.78%(6.26%)	5.81%(7.03%)	3.35%(3.67%)
	1	Residual-based (Algorithm 1)	Algorithm 7	4.33%(4.57%)	3.95%(4.31%)	4.01%(4.71%)	4.53%(5.18%)	3.78%(4.16%)	2.15%(2.78%)
Channel flow $128 \times 128 \times 1000$	1	Ridge leverage score-based (Algorithm 3)	Algorithm 4	3.91%(4.06%)	3.51%(3.47%)	3.27%(3.25%)	3.24%(3.31%)	2.35%(2.43%)	2.11%(2.17%)
	1	Ridge leverage score-based (Algorithm 3)	Algorithm 5	3.83%(3.99%)	3.43%(3.52%)	3.57%(3.93%)	3.92%(4.02%)	3.19%(3.24%)	2.55%(2.42%)
	1	Ridge leverage score-based (Algorithm 3)	Algorithm 6	4.17%(4.26%)	3.15%(3.22%)	3.21%(3.12%)	3.13%(3.22%)	1.95%(2.01%)	1.96%(2.07%)
	1	Ridge leverage score-based (Algorithm 3)	Algorithm 7	4.25%(4.35%)	3.49%(3.58%)	3.81%(3.74%)	3.75%(3.87%)	3.20%(3.37%)	2.84%(3.11%)
	Update decision			Algorithm 5	Algorithm 6	Algorithm 6	Algorithm 6	Algorithm 6	Algorithm 6
	Select best update every time			4.02%	3.54%	3.42%	3.16%	2.84%	1.96%
	2	Truncated SVD	Randomized SVD	1.76%	1.34%	0.91%	0.47%	0.34%	0.10%
	1	Randomized SVD		2.00%	1.58%	1.41%	0.83%	0.65%	0.23%
	k	CPQR	Least squares (Eq. (22))	2.67%	2.25%	2.01%	1.28%	1.04%	0.49%
	2	Leverage score	Least squares (Eq. (22))	2.89%	2.30%	2.08%	1.36%	1.17%	0.47%
Channel flow $256 \times 256 \times 1000$	2	Residual-based (Algorithm 1)	Least squares (Eq. (22))	3.12%	2.55%	2.13%	1.46%	1.32%	1.18%
	2	Ridge leverage score-based (Algorithm 3)	Least squares (Eq. (22))	3.05%	2.50%	2.21%	1.44%	1.22%	1.15%
	1	Residual-based (Algorithm 1)	Algorithm 4	3.92%(4.61%)	3.98%(4.82%)	3.52%(4.58%)	4.12%(4.36%)	4.54%(5.08%)	2.84%(3.95%)
	1	Residual-based (Algorithm 1)	Algorithm 5	3.50%(3.92%)	5.05%(5.72%)	3.27%(3.82%)	3.82%(4.81%)	3.25%(3.35%)	3.54%(4.24%)
	1	Residual-based (Algorithm 1)	Algorithm 6	4.15%(4.53%)	4.18%(4.61%)	3.71%(4.35%)	3.73%(4.72%)	2.65%(3.80%)	2.88%(3.54%)
	1	Residual-based (Algorithm 1)	Algorithm 7	3.98%(4.29%)	4.24%(4.52%)	4.05%(4.76%)	5.28%(6.10%)	2.41%(3.22%)	3.18%(3.85%)
	1	Ridge leverage score-based (Algorithm 3)	Algorithm 4	3.84%(3.96%)	3.33%(3.56%)	2.97%(3.02%)	3.31%(3.42%)	3.48%(3.57%)	2.33%(2.41%)
	1	Ridge leverage score-based (Algorithm 3)	Algorithm 5	3.21%(3.33%)	3.94%(3.76%)	2.79%(3.02%)	3.35%(3.67%)	2.85%(2.67%)	2.46%(3.04%)
	1	Ridge leverage score-based (Algorithm 3)	Algorithm 6	3.72%(3.98%)	3.18%(3.38%)	3.03%(3.65%)	3.02%(4.19%)	3.00%(3.12%)	1.76%(2.06%)
	1	Ridge leverage score-based (Algorithm 3)	Algorithm 7	3.46%(3.76%)	2.96%(3.10%)	2.85%(3.16%)	3.11%(3.72%)	1.99%(2.44%)	1.98%(2.35%)
Channel flow $256 \times 256 \times 1000$	Update decision			Algorithm 5	Algorithm 7	Algorithm 5	Algorithm 6	Algorithm 7	Algorithm 6
	Select best update every time			3.85%	2.68%	3.15%	2.77%	2.42%	1.93%
	2	Truncated SVD	Randomized SVD	1.95%	1.37%	1.01%	0.52%	0.39%	0.13%
	1	Randomized SVD		2.18%	1.82%	1.62%	0.96%	0.78%	0.29%
	k	CPQR	Least squares (Eq. (22))	2.89%	1.76%	1.55%	1.19%	0.98%	0.67%
	2	Leverage score	Least squares (Eq. (22))	2.84%	1.89%	1.69%	1.37%	0.97%	0.79%
	2	Residual-based (Algorithm 1)	Least squares (Eq. (22))	2.95%	2.17%	1.74%	1.43%	1.15%	1.27%
	2	Ridge leverage score-based (Algorithm 3)	Least squares (Eq. (22))	2.90%	1.95%	1.80%	1.39%	1.02%	0.94%
	1	Residual-based (Algorithm 1)	Algorithm 4	4.14%(4.35%)	3.54%(3.72%)	2.90%(3.71%)	2.25%(2.76%)	4.21%(4.67%)	2.97%(4.75%)
	1	Residual-based (Algorithm 1)	Algorithm 5	3.76%(4.05%)	2.86%(3.50%)	3.19%(3.92%)	2.70%(3.77%)	3.14%(4.18%)	3.51%(4.61%)
Channel flow $256 \times 256 \times 1000$	1	Residual-based (Algorithm 1)	Algorithm 6	3.98%(4.27%)	3.12%(3.79%)	2.76%(3.74%)	2.40%(3.24%)	2.06%(2.69%)	3.11%(3.52%)
	1	Residual-based (Algorithm 1)	Algorithm 7	3.74%(4.18%)	3.57%(4.15%)	2.85%(4.25%)	1.54%(1.93%)	3.10%(4.37%)	2.51%(3.17%)
	1	Ridge leverage score-based (Algorithm 3)	Algorithm 4	3.06%(3.25%)	2.92%(2.49%)	2.85%(2.93%)	2.54%(2.63%)	2.63%(2.74%)	2.39%(2.48%)
	1	Ridge leverage score-based (Algorithm 3)	Algorithm 5	3.26%(3.54%)	2.18%(2.36%)	3.19%(3.24%)	2.17%(2.07%)	2.64%(3.38%)	2.35%(2.61%)
	1	Ridge leverage score-based (Algorithm 3)	Algorithm 6	3.38%(3.72%)	2.92%(2.74%)	2.76%(2.71%)	2.24%(2.64%)	2.76%(2.84%)	2.71%(2.59%)
	1	Ridge leverage score-based (Algorithm 3)	Algorithm 7	3.04%(3.17%)	2.67%(2.13%)	2.85%(3.25%)	2.13%(1.96%)	2.92%(3.27%)	1.51%(1.98%)
	Update decision			Algorithm 7	Algorithm 5	Algorithm 6	Algorithm 7	Algorithm 6	Algorithm 7
	Select best update every time			3.28%	3.01%	2.16%	1.75%	1.42%	1.33%

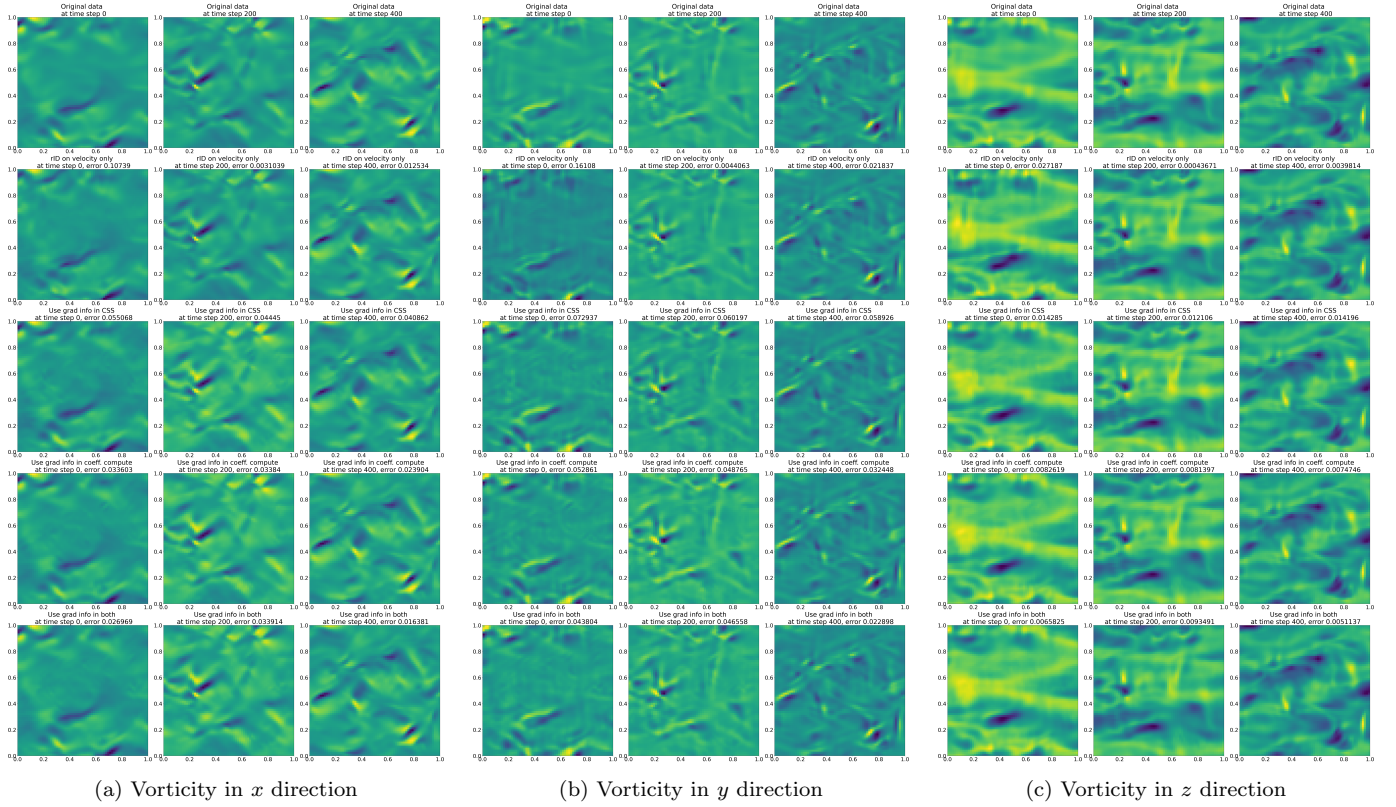


Figure 5: Rank $k = 50$, vorticity reconstruction of the turbulence flow data over a 64×64 grid at different time steps. From top to bottom: original data; randomized ID on velocity only; randomized ID with gradient information in CSS; randomized ID with gradient information in coefficient computation; and randomized ID with velocity and estimated gradient information.

Dataset	Column selection	Coeff. update criteria	Target rank					
			5	10	20	40	50	100
Channel flow $64 \times 64 \times 1000$	Only velocity term	Only velocity vector	4.02% & 11.08%	3.54% & 10.93%	3.42% & 9.64%	3.16% & 9.33%	2.84% & 9.27%	1.96% & 7.42%
	Only velocity term	With velocity gradient	4.17% & 7.83%	3.95% & 6.93%	3.87% & 6.12%	3.24% & 5.27%	3.06% & 5.19%	2.21% & 4.02%
	With velocity gradient term	Only velocity vector	3.85% & 9.32%	3.32% & 9.15%	2.97% & 8.37%	2.85% & 7.94%	2.72% & 7.32%	1.83% & 6.41%
	With velocity gradient term	With velocity gradient	3.25% & 6.25%	3.77% & 6.07%	3.64% & 5.91%	3.19% & 5.42%	2.98% & 5.01%	2.07% & 3.74%
Channel flow $128 \times 128 \times 1000$	Only velocity term	Only velocity vector	3.85% & 10.26%	3.68% & 9.92%	3.15% & 8.17%	2.77% & 7.02%	2.42% & 6.94%	1.93% & 6.81%
	Only velocity term	With velocity gradient	4.39% & 5.17%	4.15% & 5.01%	3.87% & 4.93%	3.34% & 4.77%	2.94% & 4.67%	2.19% & 4.13%
	With velocity gradient term	Only velocity vector	3.42% & 7.85%	3.17% & 6.94%	2.94% & 6.35%	2.67% & 6.01%	2.13% & 5.85%	1.78% & 5.14%
	With velocity gradient term	With velocity gradient	3.23% & 5.31%	3.35% & 5.11%	3.06% & 5.02%	2.93% & 4.95%	2.57% & 4.47%	2.08% & 3.92%
Channel flow $256 \times 256 \times 1000$	Only velocity term	Only velocity vector	3.28% & 9.02%	3.01% & 8.66%	2.16% & 8.12%	1.75% & 7.02%	1.42% & 6.98%	1.33% & 6.33%
	Only velocity term	With velocity gradient	3.84% & 5.72%	3.29% & 5.17%	2.34% & 5.01%	2.08% & 4.95%	1.87% & 4.72%	1.64% & 4.17%
	With velocity gradient term	Only velocity vector	3.15% & 7.15%	2.87% & 6.83%	2.03% & 6.35%	1.65% & 5.80%	1.22% & 5.67%	1.17% & 5.35%
	With velocity gradient term	With velocity gradient	2.90% & 5.06%	2.93% & 4.89%	2.12% & 4.75%	1.89% & 4.23%	1.45% & 4.13%	1.48% & 4.01%

Table 2: The relative error of velocity (1st value) and vorticity (2nd value) with different optimization functions and CSS criteria. The testing is performed on the turbulence channel flow dataset.

Dataset	Algorithm	Target rank					
		5	10	20	40	50	100
Channel flow $64 \times 64 \times 1000$	ID via CPQR	0.17	0.22	0.29	0.46	0.52	0.92
	Randomized SVD	0.76	1.61	1.37	2.18	3.30	3.75
	Randomized ID (Algorithm 3)	1.94	1.04	1.04	0.88	1.01	0.86
Channel flow $128 \times 128 \times 1000$	ID via CPQR	0.65	0.89	1.21	1.91	2.18	3.77
	Randomized SVD	1.55	2.56	2.96	3.62	4.21	5.08
	Randomized ID (Algorithm 3)	4.23	3.17	3.55	3.08	3.78	2.54
Channel flow $256 \times 256 \times 1000$	ID via CPQR	2.93	3.19	4.59	7.27	8.54	10.73
	Randomized SVD	3.57	7.39	9.60	10.84	13.08	16.47
	Randomized ID (Algorithm 3)	20.82	15.55	9.42	11.22	11.72	10.26

Table 3: The computational time (seconds) of compressing the channel flow dataset with different algorithms and target ranks.

4.2. Ignition dataset

In our second experiment, we evaluate the performance of our algorithm using the ignition data obtained from a jet diffusion simulation on a uniform grid of size 50×50 . In particular, the dataset is convection-dominated for the early ignition stage until the jet flame reaches a steady state. Since the flame profile changes drastically during ignition, the steady-state data cannot be well reconstructed with only the early ignition stage data, or vice versa. Therefore, the approximation accuracy is sensitive to the selection of column basis during the streaming compression and it is essential for the CSS algorithm to select the column basis containing the data in both ignition and steady-state stages. The reconstruction at several different time points is shown in Fig. 6.

Dataset	# passes	Column selection	Coeff. update	Target rank						
				5	10	20	40	50	100	
Ignition grid 50 × 50 × 450	2	Truncated SVD	Randomized SVD	9.63%	5.99%	3.06%	1.21%	0.83%	0.20%	
	1			17.7%	11.9%	8.90%	4.00%	3.09%	0.82%	
	k	CPQR	Least squares (Eq. (22))	17.45%	11.75%	7.85%	3.54%	2.52%	1.11%	
	2	Leverage score	Least squares (Eq. (22))	19.95%	14.64%	8.94%	4.19%	3.13%	2.91%	
	2	Residual-based (Algorithm 1)	Least squares (Eq. (22))	35.12%	28.73%	29.65%	18.34%	15.43%	6.19%	
	2	Ridge leverage score-based (Algorithm 3)	Least squares (Eq. (22))	20.34%	16.39%	10.74%	7.38%	4.16%	3.70%	
	1	Residual-based (Algorithm 1)	Algorithm 4	37.48%(41.23%)	30.92%(32.93%)	32.94%(34.24%)	21.20%(23.39%)	17.26%(20.64%)	7.98%(10.72%)	
	1	Residual-based (Algorithm 1)	Algorithm 5	38.10%(40.25%)	32.70%(32.16%)	33.26%(35.46%)	22.51%(24.26%)	16.98%(19.34%)	8.27%(10.54%)	
	1	Residual-based (Algorithm 1)	Algorithm 6	37.24%(39.76%)	31.83%(33.72%)	33.19%(36.75%)	20.94%(22.84%)	18.72%(23.87%)	7.15%(9.26%)	
	1	Residual-based (Algorithm 1)	Algorithm 7	36.30%(39.69%)	30.80%(33.25%)	32.09%(33.34%)	22.64%(23.54%)	19.05%(22.34%)	8.93%(10.39%)	
	1	Ridge leverage score-based (Algorithm 3)	Algorithm 4	25.26%(27.13%)	21.81%(22.15%)	13.36%(14.97%)	9.32%(10.16%)	5.92%(6.03%)	4.85%(5.03%)	
	1	Ridge leverage score-based (Algorithm 3)	Algorithm 5	28.10%(29.54%)	23.69%(26.37%)	13.76%(14.86%)	10.51%(11.37%)	4.98%(5.34%)	3.91%(4.28%)	
	1	Ridge leverage score-based (Algorithm 3)	Algorithm 6	27.16%(28.93%)	24.17%(26.92%)	13.79%(13.85%)	11.98%(12.85%)	5.17%(7.18%)	4.93%(5.44%)	
	1	Ridge leverage score-based (Algorithm 3)	Algorithm 7	23.19%(24.73%)	20.84%(21.42%)	12.40%(13.54%)	10.64%(12.49%)	5.35%(6.24%)	3.75%(3.76%)	
	Update decision				Algorithm 7	Algorithm 7	Algorithm 7	Algorithm 4	Algorithm 5	Algorithm 7
	Select best update every time (Algorithm 3)				24.31%	19.64%	12.52%	9.35%	4.82%	3.94%

Table 4: The relative error of randomized ID with different coefficient computation algorithms and different numbers of new columns. The estimated error using single-pass Hutch++ is included in the bracket. The testing is performed on the ignition database.

In Table 4, we measure the effect of the target rank k on the relative error of different coefficient computation algorithms and use the truncated SVD and single-pass randomized SVD [13] as the benchmark for comparison. From the last row of each category in Table 4, we still find that the reconstruction accuracy keeps improving when the target size increases. In terms of different coefficient algorithms, we find the reconstruction accuracy depends on the target rank setting and we cannot find an algorithm that beats the rest in every target rank. In addition, the Hutch++ error estimator still predicts the Frobenius error accurately and determines the coefficient matrix that produces a smaller reconstruction error.

Dataset	Algorithm	Target rank					
		5	10	20	40	50	100
Ignition grid $50 \times 50 \times 450$	ID via CPQR	0.08	0.10	0.13	0.23	0.23	0.25
	Randomized SVD	0.23	0.28	0.48	0.51	0.70	1.02
	Randomized ID (Algorithm 3)	2.71	1.77	1.19	1.27	0.79	0.35

Table 5: The computational time (seconds) of compressing the ignition dataset with different algorithms and target ranks.

Regarding the performance of the ridge leverage score-based CSS algorithm, we first compare it with other CSS methods in a two-pass setting. We observe similar results as in the channel flow dataset in that the CSS based on ridge leverage score (Algorithm 3) performs slightly worse than the standard leverage score CSS and both methods perform slightly worse than the CPQR method. However, both methods perform significantly better than the residual-based CSS (Algorithm 1). A possible reason for the poor performance of the residual-based CSS (Algorithm 1) is that it cannot prune the already selected column basis and therefore fails to preserve the key time frames in the later stages of the dataset. Instead, the ridge leverage score-based method (3) performs sampling among the entire data matrix and thus can effectively handle the dataset with a large number of time steps. We then compare the ridge leverage score-based CSS (Algorithm 3) with the residual-based CSS (Algorithm 1) in an online setting where the coefficient matrix is computed simultaneously with CSS. We observe that the ridge leverage score-based method outperforms the residual-based CSS method, which verifies the ability of our framework to handle datasets with drastic temporal variations.

In Table 5, we also compare the runtime of our online randomized ID method with the offline ID via CPQR and the online randomized SVD [13]. Similar to the result in the channel flow dataset, we find that the computational time of our randomized ID method (3) decreases along with the target rank. The offline ID method is generally faster than the two online algorithms because the small dataset can be easily loaded into RAM for multiple accesses. However, the computational time of our approach is still comparable when the target rank is larger. Compared to the single-pass randomized SVD, our method is faster when the target rank is large but is less accurate (Table 4).

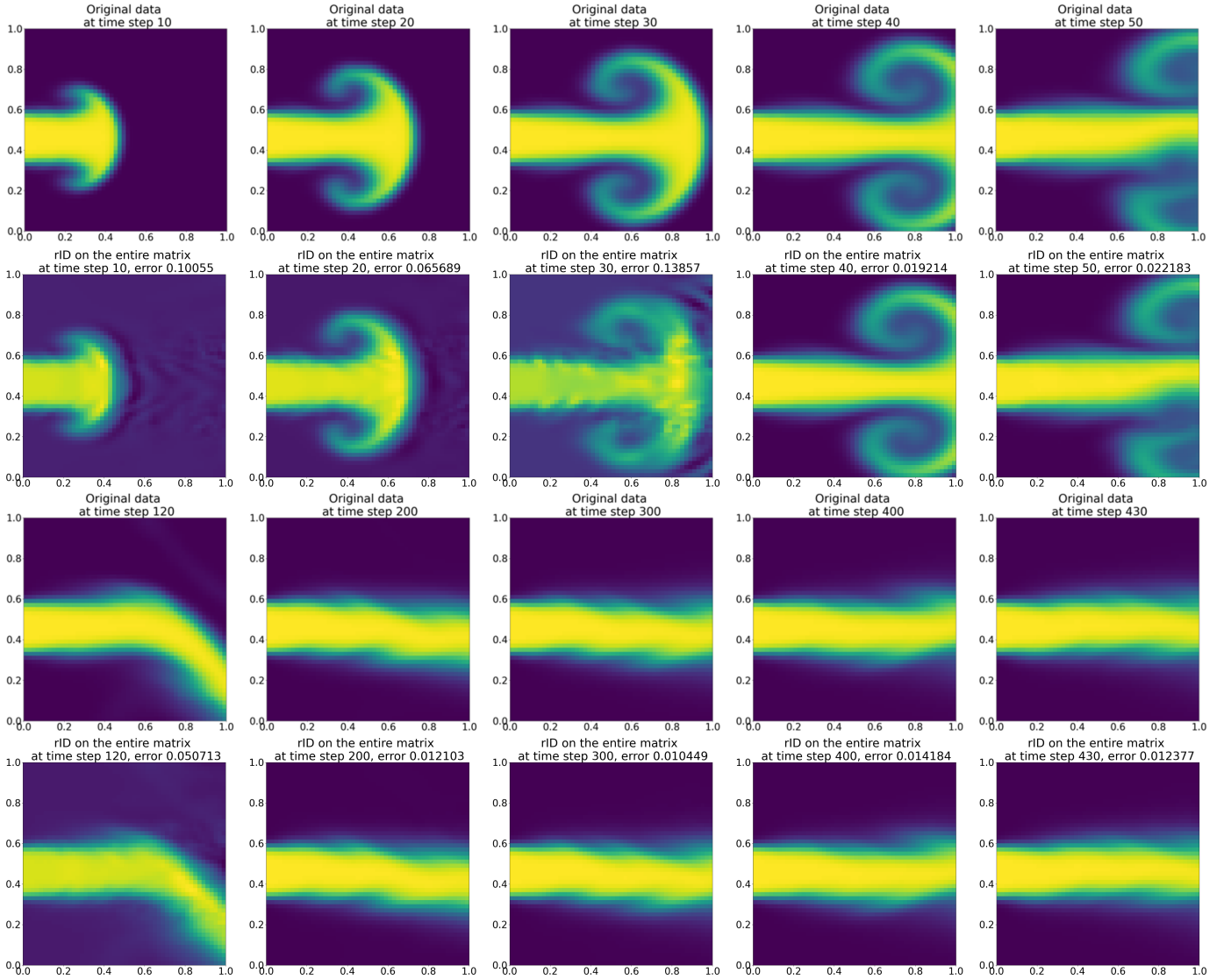


Figure 6: Rank $k = 40$ reconstruction of ignition data on a grid of size 50×50 at different time steps. For each two rows, the top one represents the original data while the bottom one represents the reconstruction data.

4.3. The NSTX Gas Puff Image (GPI) data

In the previous two tests, the input data matrix $m \times n$ data matrix \mathbf{A} satisfies $m \gg n$. To evaluate the performance of our online framework in handling the datasets with many time steps ($n \gg m$), we next consider the NSTX GPI dataset [28, 29] that contains 369,357 data snapshots over a grid of size 80×64 . Since the dataset was obtained from an experiment, the first half of the time points are used to calibrate the measurement noise. Here, we compute the average of the first 169,357 frames as the baseline noise which we subtract from the entire dataset. Then, we use the remaining 200,000 frames as the input data to our framework. The reconstructed data with target rank $k = 100$ at different time steps is shown in Fig. 7. We find that the reconstruction result effectively preserves the profile of the gas puff. In particular, we find that the original data at the initial time steps (5,000 and 25,000) is still noisy and the gas puff profile is hard to identify. However, the reconstruction manages to reduce the noise signal, demonstrating that our randomized ID method captures the key time frames as column bases for compression.

In Table 6, we monitor the reconstruction accuracy during the streaming data process and summarize the accuracy at four different time steps: 50,000, 100,000, 150,000, and 200,000. For each

Dataset	# passes	Column selection	Coeff. update	Target rank			
				100	200	400	800
NSTX GPI data $80 \times 64 \times 50,000$	2	Truncated SVD		8.78%	8.17%	7.61%	6.95%
	1	Randomized SVD		10.12%	9.35%	7.91%	7.35%
	k	CPQR	Least squares (Eq. (22))	10.52%	9.75%	7.85%	6.54%
	2	Leverage score	Least squares (Eq. (22))	13.17%	11.42%	8.96%	7.97%
	2	Residual-based (Algorithm 1)	Least squares (Eq. (22))	36.34%	30.56%	19.16%	12.31%
	2	Ridge leverage score-based (Algorithm 3)	Least squares (Eq. (22))	11.25%	9.54%	9.12%	8.54%
	1	Residual-based (Algorithm 1)	Algorithm 4	39.71%(40.16%)	32.54% (34.83%)	22.63% (21.53%)	16.12%(19.62%)
	1	Residual-based (Algorithm 1)	Algorithm 5	38.96%(39.81%)	33.78%(31.58%)	25.13%(27.24%)	20.83% (17.34%)
	1	Residual-based (Algorithm 1)	Algorithm 6	38.87%(37.65%)	34.62%(34.67%)	22.95%(23.75%)	16.14%(21.87%)
	1	Residual-based (Algorithm 1)	Algorithm 7	37.79% (36.10%)	33.02%(32.17%)	24.24%(23.64%)	16.05%(20.34%)
	1	Ridge leverage score-based (Algorithm 3)	Algorithm 4	13.12%(14.21%)	11.24%(11.39%)	9.36%(9.53%)	8.51% (8.12%)
	1	Ridge leverage score-based (Algorithm 3)	Algorithm 5	12.91% (13.21%)	11.43%(11.52%)	9.57%(10.27%)	8.92%(9.25%)
	1	Ridge leverage score-based (Algorithm 3)	Algorithm 6	13.25%(13.47%)	11.49%(11.58%)	9.81%(10.46%)	8.64%(8.37%)
	1	Ridge leverage score-based (Algorithm 3)	Algorithm 7	13.17%(13.59%)	11.15% (11.22%)	9.28% (9.31%)	8.77%(8.39%)
	Update decision			Algorithm 5	Algorithm 7	Algorithm 7	Algorithm 4
	Select best update every time (Algorithm 3)			12.38%	10.45%	8.99%	7.99%
NSTX GPI data $80 \times 64 \times 100,000$	2	Truncated SVD		11.33%	10.66%	9.99%	9.18%
	1	Randomized SVD		12.84%	11.74%	10.65%	10.12%
	k	CPQR	Least squares (Eq. (22))	12.92%	11.35%	10.52%	9.03%
	2	Leverage score	Least squares (Eq. (22))	13.74%	13.63%	12.08%	9.37%
	2	Residual-based (Algorithm 1)	Least squares (Eq. (22))	37.43%	31.74%	23.65%	14.91%
	2	Ridge leverage score-based (Algorithm 3)	Least squares (Eq. (22))	13.64%	11.93%	11.21%	9.89%
	1	Residual-based (Algorithm 1)	Algorithm 4	38.74%(39.62%)	32.50%(34.13%)	26.63% (26.81%)	19.12%(20.34%)
	1	Residual-based (Algorithm 1)	Algorithm 5	36.66%(35.18%)	31.54% (31.29%)	29.13%(29.42%)	23.83% (21.75%)
	1	Residual-based (Algorithm 1)	Algorithm 6	37.25%(37.24%)	33.21%(32.70%)	26.95%(27.98%)	20.42%(24.78%)
	1	Residual-based (Algorithm 1)	Algorithm 7	35.79% (34.59%)	32.40%(33.33%)	28.24%(28.90%)	20.30%(22.34%)
	1	Ridge leverage score-based (Algorithm 3)	Algorithm 4	15.15%(15.37%)	14.50%(16.13%)	13.13%(13.97%)	11.12%(11.96%)
	1	Ridge leverage score-based (Algorithm 3)	Algorithm 5	16.32%(16.21%)	13.54% (14.29%)	11.63% (11.81%)	10.83% (10.34%)
	1	Ridge leverage score-based (Algorithm 3)	Algorithm 6	15.58%(14.90%)	14.21%(16.70%)	11.95%(12.98%)	11.02%(10.78%)
	1	Ridge leverage score-based (Algorithm 3)	Algorithm 7	14.79% (14.30%)	15.40%(15.33%)	12.24%(13.12%)	11.30%(11.54%)
	Update decision			Algorithm 7	Algorithm 5	Algorithm 5	Algorithm 5
	Select best update every time (Algorithm 3)			14.47%	12.77%	11.48%	10.45%
NSTX GPI data $80 \times 64 \times 150,000$	2	Truncated SVD		13.36%	12.64%	11.88%	10.94%
	1	Randomized SVD		14.31%	13.24%	12.16%	11.75%
	k	CPQR	Least squares (Eq. (22))	14.95%	13.11%	12.38%	11.37%
	2	Leverage score	Least squares (Eq. (22))	17.58%	15.62%	14.69%	12.37%
	2	Residual-based (Algorithm 1)	Least squares (Eq. (22))	39.76%	32.39%	25.69%	17.14%
	2	Ridge leverage score-based (Algorithm 3)	Least squares (Eq. (22))	15.12%	13.95%	12.54%	11.96%
	1	Residual-based (Algorithm 1)	Algorithm 4	42.12%(43.13%)	37.24%(36.29%)	31.16%(30.90%)	18.29%(19.16%)
	1	Residual-based (Algorithm 1)	Algorithm 5	43.62%(43.23%)	36.10% (37.12%)	30.31%(30.42%)	19.75% (20.19%)
	1	Residual-based (Algorithm 1)	Algorithm 6	42.25%(42.57%)	38.21%(38.16%)	29.75%(31.98%)	21.62%(22.91%)
	1	Residual-based (Algorithm 1)	Algorithm 7	41.79% (42.01%)	39.41%(37.73%)	29.63% (29.81%)	21.83%(21.45%)
	1	Ridge leverage score-based (Algorithm 3)	Algorithm 4	17.17%(18.30%)	15.95%(15.12%)	14.05%(14.30%)	13.39%(14.81%)
	1	Ridge leverage score-based (Algorithm 3)	Algorithm 5	17.26%(18.14%)	14.18% (14.30%)	14.19%(14.44%)	13.17%(14.07%)
	1	Ridge leverage score-based (Algorithm 3)	Algorithm 6	17.38%(17.72%)	14.92%(14.74%)	13.76% (13.92%)	13.24%(13.64%)
	1	Ridge leverage score-based (Algorithm 3)	Algorithm 7	17.04% (17.17%)	14.67%(14.83%)	14.85%(14.25%)	13.13% (12.96%)
	Update decision			Algorithm 7	Algorithm 5	Algorithm 6	Algorithm 7
	Select best update every time (Algorithm 3)			16.28%	14.65%	13.45%	12.37%
NSTX GPI data $80 \times 64 \times 200,000$	2	Truncated SVD		14.98%	14.19%	13.34%	12.29%
	1	Randomized SVD		16.35%	15.06%	14.35%	13.15%
	k	CPQR	Least squares (Eq. (22))	14.15%	15.13%	14.24%	12.77%
	2	Leverage score	Least squares (Eq. (22))	17.26%	17.32%	15.25%	12.11%
	2	Residual-based (Algorithm 1)	Least squares (Eq. (22))	40.59%	33.83%	26.02%	18.35%
	2	Ridge leverage score-based (Algorithm 3)	Least squares (Eq. (22))	16.90%	15.05%	14.51%	13.16%
	1	Residual-based (Algorithm 1)	Algorithm 4	39.86% (40.11%)	34.97%(35.62%)	26.11% (27.94%)	19.95%(21.76%)
	1	Residual-based (Algorithm 1)	Algorithm 5	43.62%(44.78%)	34.10% (33.29%)	27.31%(29.64%)	20.83%(21.35%)
	1	Residual-based (Algorithm 1)	Algorithm 6	41.25%(42.49%)	34.66%(34.57%)	26.75%(27.83%)	20.62%(22.17%)
	1	Residual-based (Algorithm 1)	Algorithm 7	42.71%(43.26%)	35.91%(35.36%)	28.85%(29.97%)	19.07% (20.38%)
	1	Ridge leverage score-based (Algorithm 3)	Algorithm 4	18.33%(18.25%)	17.32%(18.74%)	15.23%(16.39%)	14.94%(14.81%)
	1	Ridge leverage score-based (Algorithm 3)	Algorithm 5	18.94%(18.13%)	17.34% (17.56%)	15.84%(16.13%)	14.73%(15.17%)
	1	Ridge leverage score-based (Algorithm 3)	Algorithm 6	18.81%(18.24%)	17.23%(17.91%)	15.13% (15.96%)	14.85%(15.29%)
	1	Ridge leverage score-based (Algorithm 3)	Algorithm 7	18.24% (17.87%)	17.16%(17.93%)	15.39%(16.29%)	14.32% (14.52%)
	Update decision			Algorithm 7	Algorithm 5	Algorithm 6	Algorithm 7
	Select best update every time (Algorithm 3)			18.00%	16.95%	15.11%	13.93%

Table 6: The relative error of randomized ID with different coefficient computation algorithms and different numbers of new columns. The estimated error using single-pass Hutch++ is included in the bracket. Testing is performed on NSTX Gas Puff Image Data after denoising.

case, we measure the effect of the target rank (k) coefficient computation algorithm on the relative error and use the SVD and a single-pass randomized SVD as the benchmarks for comparison. Similar to the previous results, the reconstruction accuracy keeps improving as the target rank increases. In

Dataset	Algorithm	Target rank			
		100	200	400	800
$80 \times 64 \times 50,000$	ID via CPQR	55.7	104.4	198.5	384.9
	Randomized SVD	19.1	30.8	46.7	51.6
	Randomized ID (Algorithm 3)	32.1	46.4	74.2	103.7
$80 \times 64 \times 100,000$	ID via CPQR	129.6	253.4	497.3	937.2
	Randomized SVD	36.3	42.9	75.2	97.1
	Randomized ID (Algorithm 3)	50.7	72.6	94.3	143.2
$80 \times 64 \times 150,000$	ID via CPQR	207.3	398.4	802.1	1542.3
	Randomized SVD	52.2	76.6	105.9	156.7
	Randomized ID (Algorithm 3)	73.4	94.8	119.9	192.6
$80 \times 64 \times 200,000$	ID via CPQR	294.1	601.7	1312.6	2517.3
	Randomized SVD	79.8	102.3	135.8	231.8
	Randomized ID (Algorithm 3)	96.3	125.9	172.3	351.4

Table 7: The computational time (seconds) of compressing the NSTX Gas Puff Image dataset with different algorithms and target ranks.

addition, no single coefficient calculation strategy leads to more accurate reconstructions uniformly across the ranks, and the NA-Hutch++ scheme produces accurate error estimates. By selecting the best updating algorithm via the NA-Hutch++ error estimator, whenever the column basis is updated, we obtain more accurate reconstructions than using a single coefficient computation algorithm.

Regarding the performance of the ridge leverage score-based CSS algorithm, we first compare it with other CSS methods in a two-pass setting. We observe similar results as in the channel flow dataset where the CSS method performs slightly worse than the standard leverage score CSS [37] and both leverage score-based CSS methods perform slightly worse than the CPQR method. And as before, both leverage score-based methods perform significantly better than the residual-based CSS. By comparing our choice of CSS method with the residual-based CSS in a single-pass setting, we similarly observe that the ridge leverage score-based method outperforms the residual-based CSS method, which demonstrates the ability of our approach to handle a dataset consisting of many time frames.

In Table 7, we also compare the runtime of our online randomized ID method with the offline ID via CPQR and the online randomized SVD [13]. We find that the computational time of our method increases along with the target rank, unlike in the previous two experiments. A possible reason is that, due to the larger column size of the dataset, the computation of the coefficients dominates the compression process and thus offsets the efficiency improvement of the CSS process by allowing more columns stored in RAM. Though the offline ID method is generally faster compared to the two online algorithms, our method achieves a comparable computational time when the target rank is large. As compared to the single-pass randomized SVD method, our approach obtains comparable reconstruction accuracy with much less computational time when the target rank is large (Table 6). The reason is that the larger column size of the dataset significantly increases the frequency of SVD updates and thus increases the overall computation time. Overall, our proposed method performs well in handling a dataset with larger snapshots in terms of accuracy and computational cost.

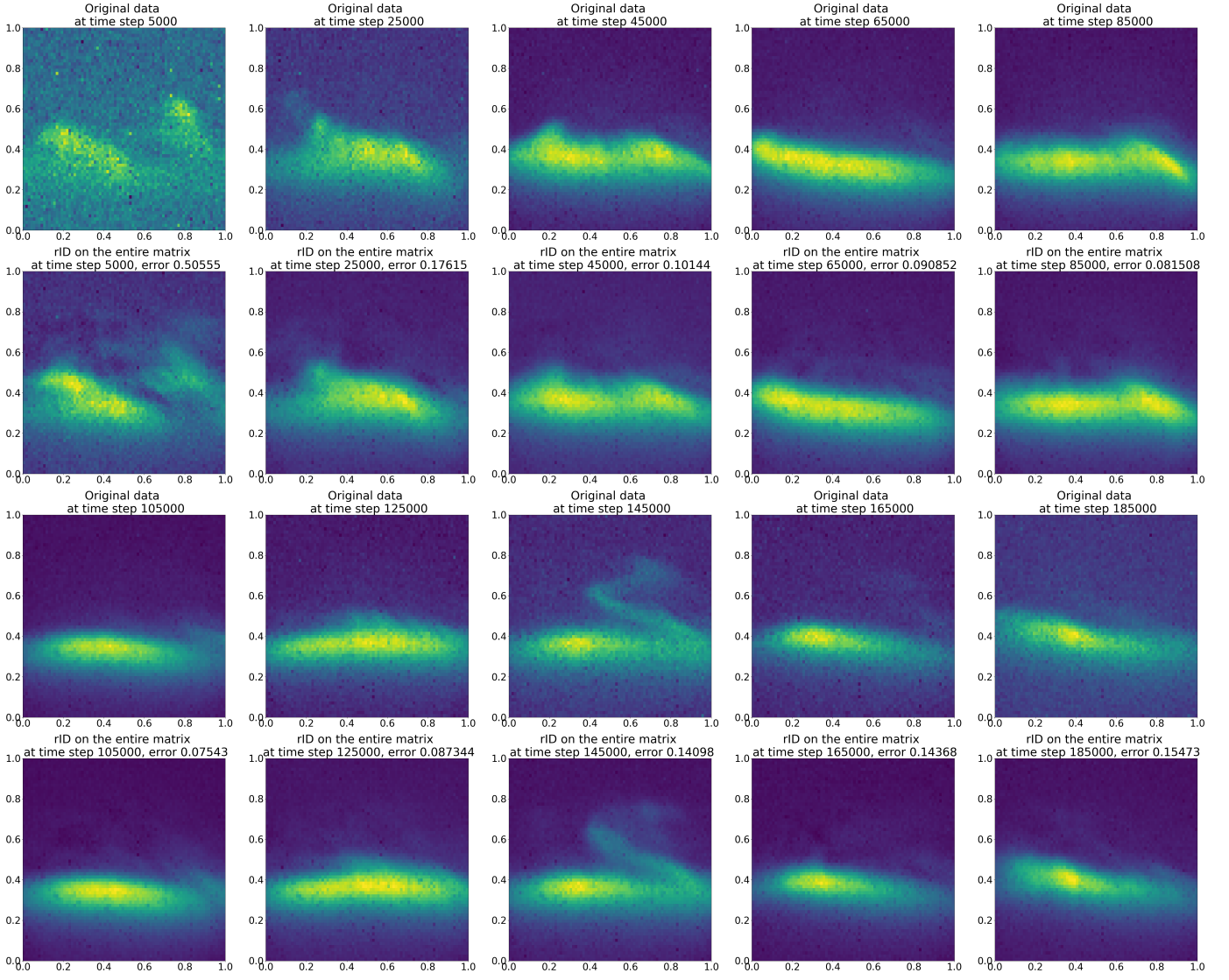


Figure 7: Rank $k = 100$ reconstruction of NSTX gas puff image data over a grid of size 80×64 at different time instances. For each two rows, the top one represents the original data while the bottom one represents the reconstruction data.

5. Conclusions

In this study, we develop a randomized ID approach to perform temporal compression in a single pass over large-scale, streaming simulation data. We first implement a streaming ridge leverage score-based CSS method to pick the column basis (a subset of data snapshots) for decomposition. As more data is observed, we evolve the column basis and accordingly update the coefficient matrix completing the decomposition. We utilize randomized projection to generate a data sketch that can fit within the main memory. Four different strategies for coefficient calculation are considered that differ in using the full or sketched data to approximate the least squares solution. To pick the best coefficient matrix, we rely on an estimate of the reconstruction error generated via the NA-Hutch++ method. We show that the proposed algorithms can be employed to obtain the low-rank approximation of data taken from (1) a 3D turbulent channel flow; (2) a 2D ignition problem; and (3) the NSTX Gas Puff Image (GPI) measurements. We also present an adaptation of the single-pass, randomized ID method that results in improving the reconstruction error of the solution gradient, when desired, without losing considerable accuracy on the reconstructed solution itself.

Future extensions of the proposed strategy include parallel, *in situ* implementation in conjunction

with the PDE solver generating solution data. In addition, the current rank-based implementation can be altered to an error-based formulation where the solution rank is increased to achieve a prescribed accuracy, is attainable. Last but not least, the proposed temporal compression can be augmented with spatial compression by utilizing spatial compressors, such as SZ [38] and FPZIP [39], to reduce the column basis vectors, thereby achieving higher compression factors.

Acknowledgements

This material is based upon work supported by the Department of Energy Advanced Scientific Computing Research Award DE-SC0022283. AD’s work has also been partially supported by AFOSR grant FA9550-20-1-0138 and SB’s work has been partially supported by DOE award DE-SC0023346. We would also like to thank Kenneth Jansen, John Evans, and Jeff Hadley from the University of Colorado Boulder for their helpful discussions surrounding this work.

Declaration of competing interest

The authors declare that they have no known competing financial interests or personal relationships that could have appeared to influence the work reported in this paper.

References

- [1] C. Eckart, G. Young, The approximation of one matrix by another of lower rank, *Psychometrika* 1 (3) (1936) 211–218.
- [2] R. Saha, V. Srivastava, M. Pilanci, Matrix compression via randomized low rank and low precision factorization, in: A. Oh, T. Naumann, A. Globerson, K. Saenko, M. Hardt, S. Levine (Eds.), *Advances in Neural Information Processing Systems*, Vol. 36, Curran Associates, Inc., 2023, pp. 18828–18872.
- [3] S. Voronin, P.-G. Martinsson, Efficient algorithms for cur and interpolative matrix decompositions, *Advances in Computational Mathematics* 43 (2017) 495–516.
- [4] A. M. Dunton, L. Jofre, G. Iaccarino, A. Doostan, Pass-efficient methods for compression of high-dimensional turbulent flow data, *Journal of Computational Physics* 423 (2020) 109704.
- [5] H. Pacella, A. Dunton, A. Doostan, G. Iaccarino, Task-parallel in situ temporal compression of large-scale computational fluid dynamics data, *The International Journal of High Performance Computing Applications* 36 (3) (2022) 388–418.
- [6] X.-M. Pan, J.-G. Wei, Z. Peng, X.-Q. Sheng, A fast algorithm for multiscale electromagnetic problems using interpolative decomposition and multilevel fast multipole algorithm, *Radio Science* 47 (01) (2012) 1–11.
- [7] S.-L. Huang, H. Xu, X.-M. Pan, X.-Q. Sheng, Efficient mpi parallel interpolative decomposition, in: *2016 IEEE International Conference on Microwave and Millimeter Wave Technology (ICMMT)*, Vol. 2, IEEE, 2016, pp. 807–809.
- [8] J. Hampton, H. R. Fairbanks, A. Narayan, A. Doostan, Practical error bounds for a non-intrusive bi-fidelity approach to parametric/stochastic model reduction, *Journal of Computational Physics* 368 (2018) 315–332.

- [9] R. W. Skinner, A. Doostan, E. L. Peters, J. A. Evans, K. E. Jansen, Reduced-basis multifidelity approach for efficient parametric study of naca airfoils, *AIAA Journal* 57 (4) (2019) 1481–1491.
- [10] H. R. Fairbanks, L. Jofre, G. Geraci, G. Iaccarino, A. Doostan, Bi-fidelity approximation for uncertainty quantification and sensitivity analysis of irradiated particle-laden turbulence, *Journal of Computational Physics* 402 (2020) 108996.
- [11] E. Liberty, F. Woolfe, P.-G. Martinsson, V. Rokhlin, M. Tygert, Randomized algorithms for the low-rank approximation of matrices, *Proceedings of the National Academy of Sciences* 104 (51) (2007) 20167–20172.
- [12] N. Halko, P.-G. Martinsson, J. A. Tropp, Finding structure with randomness: Probabilistic algorithms for constructing approximate matrix decompositions, *SIAM Review* 53 (2) (2011) 217–288.
- [13] W. Yu, Y. Gu, J. Li, S. Liu, Y. Li, Single-pass PCA of large high-dimensional data, *arXiv preprint arXiv:1704.07669* (2017).
- [14] C. Boutsidis, M. W. Mahoney, P. Drineas, An improved approximation algorithm for the column subset selection problem, in: *Proceedings of the twentieth annual ACM-SIAM symposium on Discrete algorithms*, SIAM, 2009, pp. 968–977.
- [15] C. Boutsidis, P. Drineas, M. Magdon-Ismail, Near-optimal column-based matrix reconstruction, *SIAM Journal on Computing* 43 (2) (2014) 687–717.
- [16] A. Deshpande, L. Rademacher, Efficient volume sampling for row/column subset selection, in: *2010 IEEE 51st Annual Symposium on Foundations of Computer Science*, IEEE, 2010, pp. 329–338.
- [17] S. Paul, M. Magdon-Ismail, P. Drineas, Column selection via adaptive sampling, *Advances in neural information processing systems* 28 (2015).
- [18] J. A. Tropp, Column subset selection, matrix factorization, and eigenvalue optimization, in: *Proceedings of the twentieth annual ACM-SIAM symposium on Discrete algorithms*, SIAM, 2009, pp. 978–986.
- [19] M. W. Mahoney, et al., Randomized algorithms for matrices and data, *Foundations and Trends® in Machine Learning* 3 (2) (2011) 123–224.
- [20] A. Civril, M. Magdon-Ismail, Column subset selection via sparse approximation of SVD, *Theoretical Computer Science* 421 (2012) 1–14.
- [21] M. B. Cohen, C. Musco, C. Musco, Input sparsity time low-rank approximation via ridge leverage score sampling, in: *Proceedings of the Twenty-Eighth Annual ACM-SIAM Symposium on Discrete Algorithms*, SIAM, 2017, pp. 1758–1777.
- [22] A. Bhaskara, S. Lattanzi, S. Vassilvitskii, M. Zadimoghaddam, Residual based sampling for online low rank approximation, in: *2019 IEEE 60th Annual Symposium on Foundations of Computer Science (FOCS)*, IEEE, 2019, pp. 1596–1614.
- [23] R. A. Meyer, C. Musco, C. Musco, D. P. Woodruff, Hutch++: Optimal stochastic trace estimation, in: *Symposium on Simplicity in Algorithms (SOSA)*, SIAM, 2021, pp. 142–155.

- [24] E. Perlman, R. Burns, Y. Li, C. Meneveau, Data exploration of turbulence simulations using a database cluster, in: Proceedings of the 2007 ACM/IEEE Conference on Supercomputing, 2007, pp. 1–11.
- [25] Y. Li, E. Perlman, M. Wan, Y. Yang, C. Meneveau, R. Burns, S. Chen, A. Szalay, G. Eyink, A public turbulence database cluster and applications to study lagrangian evolution of velocity increments in turbulence, *Journal of Turbulence* (9) (2008) N31.
- [26] J. Graham, K. Kanov, X. Yang, M. Lee, N. Malaya, C. Lalescu, R. Burns, G. Eyink, A. Szalay, R. Moser, et al., A web services accessible database of turbulent channel flow and its use for testing a new integral wall model for les, *Journal of Turbulence* 17 (2) (2016) 181–215.
- [27] J. Choi, R. Wang, R. M. Churchill, R. Kube, M. Choi, J. Park, J. Logan, K. Mehta, G. Eisenhauer, N. Podhorszki, et al., Data federation challenges in remote near-real-time fusion experiment data processing, in: Driving Scientific and Engineering Discoveries Through the Convergence of HPC, Big Data and AI: 17th Smoky Mountains Computational Sciences and Engineering Conference, SMC 2020, Oak Ridge, TN, USA, August 26-28, 2020, Revised Selected Papers 17, Springer, 2020, pp. 285–299.
- [28] K. Zhao, S. Di, X. Lian, S. Li, D. Tao, J. Bessac, Z. Chen, F. Cappello, Sdrbench: Scientific data reduction benchmark for lossy compressors, in: 2020 IEEE international conference on big data (Big Data), IEEE, 2020, pp. 2716–2724.
- [29] SDRBench, <https://sdrbench.github.io>.
- [30] M. Ghashami, E. Liberty, J. M. Phillips, D. P. Woodruff, Frequent directions: Simple and deterministic matrix sketching, *SIAM Journal on Computing* 45 (5) (2016) 1762–1792.
- [31] M. Pilanci, M. J. Wainwright, Iterative hessian sketch: Fast and accurate solution approximation for constrained least-squares, *Journal of Machine Learning Research* 17 (53) (2016) 1–38.
- [32] S. Becker, B. Kawas, M. Petrik, Robust partially-compressed least-squares, in: Proceedings of the AAAI Conference on Artificial Intelligence, Vol. 31, 2017.
- [33] M. F. Hutchinson, A stochastic estimator of the trace of the influence matrix for laplacian smoothing splines, *Communications in Statistics-Simulation and Computation* 18 (3) (1989) 1059–1076.
- [34] K. L. Clarkson, D. P. Woodruff, Numerical linear algebra in the streaming model, in: Proceedings of the forty-first annual ACM symposium on Theory of computing, 2009, pp. 205–214.
- [35] D. M. Bortz, C. T. Kelley, [The Simplex Gradient and Noisy Optimization Problems](#), Birkhäuser Boston, Boston, MA, 1998, pp. 77–90. doi:10.1007/978-1-4612-1780-0_5. URL https://doi.org/10.1007/978-1-4612-1780-0_5
- [36] G. H. Golub, M. Heath, G. Wahba, Generalized cross-validation as a method for choosing a good ridge parameter, *Technometrics* 21 (2) (1979) 215–223.
- [37] I. T. Jolliffe, Discarding variables in a principal component analysis. i: Artificial data, *Journal of the Royal Statistical Society Series C: Applied Statistics* 21 (2) (1972) 160–173.
- [38] S. Di, F. Cappello, Fast error-bounded lossy hpc data compression with sz, in: 2016 IEEE international parallel and distributed processing symposium (ipdps), IEEE, 2016, pp. 730–739.

- [39] P. Lindstrom, M. Isenburg, Fast and efficient compression of floating-point data, *IEEE transactions on visualization and computer graphics* 12 (5) (2006) 1245–1250.